

DDC FILE COPY AD 606871

15

RADC-TDR-64-244 ✓
Final Report

4915-2-F



A STUDY OF PLASMA APPLICATIONS
IN MICROWAVE CIRCUITS-II

4915-2-F = RL-2118

TECHNICAL DOCUMENTARY REPORT NO. RADC-TDR-64-244
August 1964

Techniques Branch
Rome Air Development Center
Research and Technology Division
Air Force Systems Command
Griffiss Air Force Base, New York

Project No. 5573 , Task No. 557301

(Prepared under Contract No. AF 30(602)-2605 by A. Olte and E.K. Miller, The University of Michigan, College of Engineering, Department of Electrical Engineering, Radiation Laboratory.)

DDC
RECEIVED
OCT 16 1964
RECEIVED
DEPT. OF DEFENSE

ELECTRON PHYSICS LAB.

FOREWORD

The assistance of Kenneth L. Young in carrying out the experimental part of this investigation is gratefully acknowledged. Mr. David Myers was extremely helpful with suggestions and his skill in building the glass envelope for the discharge tube was invaluable. Our thanks are due Mr. V.R. Burris and Mr. James Murphy of the Electron Physics Laboratory of The University for their useful suggestions and for the use of their equipment, and to the engineers of the General Electric Company Tube Division at Owensboro, Kentucky for the advice and materials which they provided. We are also grateful for the help and support of Ralph E. Hiatt.

4915-2-F

ABSTRACT

A continuation of previous work in this laboratory (Olte, Miller, 1963) is reported. These studies are concerned with the potential usefulness of plasmas in microwave structures, with or without a static magnetic field. Both efforts had as their main goals the study of plasmas and microwave configurations that appear to have promise as useful plasma devices. In the present study considerable attention has been given to the plasma resonance isolator and to the design and fabrication of an improved plasma package specifically intended for microwave applications.

The first part of the report contains the development of a first order theory for calculating the absorption in the electron cyclotron resonance isolator, and its equivalent circuit. Two theoretical models are used to describe the plasma-electromagnetic wave interaction and are found to produce equivalent results for the range of variables investigated. A comparison of theoretical and experimental results shows the theory to be reasonable when the assumptions which are made in its development are satisfied by the experimental conditions.

The experimental work on a rectangular plasma package is described in the second part of the report. Hydrogen and xenon gases are used in hot cathode discharges to produce a plasma, and plasma frequencies of more than 10 Gc are obtained. Plasma instabilities were found to be a serious problem.

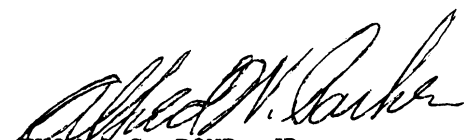
PUBLICATION REVIEW

This report has been reviewed and is approved. For further technical information on this project, contact EMATE, Joseph M. Schenna, X4251

Approved:


JOSEPH M. SCHENNA
Project Engineer
Electron Devices Section

Approved:


THOMAS S. BOND, JR.
Colonel, USAF
Chief, Surveillance and
Control Division

FOR THE COMMANDER:


IRVING J. GABELMAN
Chief, Advanced Studies Group

TABLE OF CONTENTS

I	Introduction	1
	Present Uses for Plasmas	4
	Possible Plasma Applications	6
II	Theoretical Derivation of Absorption in the Electron Cyclotron Resonance Isolator and Its Equivalent Circuit	10
	The Tensor Model	12
	The Equivalent Scalar Model	15
	Isolator Absorption Formulae	17
	Comparison with Experimental Measurements	30
	Equivalent Circuit of the Cyclotron Resonance Isolator	37
III	Experimental Work on Plasma Package	42
	Introduction	42
	Experimental Results	45
	Hydrogen Discharge	55
	Xenon Discharge	66
IV	Conclusions	77
	References	79

LIST OF ILLUSTRATIONS

Nr.	Title	Page
II-1	Sketch of Isolator	11
II-2	PTC as Function of Y Calculated from Extraordinary Wave Approximation	19
II-3	PTC as Function of Frequency Calculated from Extraordinary Wave Approximation with Elliptical Polarization Accounted for and Parabolic Magnetic Field Variation	26
II-4	PTC as Function of Frequency Calculated for Tensor Permittivity and Parabolic Magnetic Field Variation	27
II-5	PTC as Function of Y_0 Calculated from Extraordinary Wave Approximation with Elliptic Polarization Accounted for and Parabolic Magnetic Field Variation	28
II-6	PTC as Function of Y_0 Calculated for Tensor Permittivity and Parabolic Magnetic Field Variation	29
II-7	Relative Decrease in Minimum PTC as Function of Magnetic Field Variation over Plasma Volume for both Equivalent Scalar Permittivity and Tensor Permittivity	31
II-8	No Plasma Isolator Insertion Loss without Mode Suppressors	32
II-9	Experimental and Theoretical Power Transmission as Function of Frequency. Calculated from Tensor Permittivity and Parabolic Magnetic Field Variation	33
II-10	Experimental and Theoretical Power Transmission as Function of Frequency	34
II-11	Experimental and Theoretical Power Transmission Coefficient as Function of Y_0	35
II-12	Electron Cyclotron Resonance Isolator and Its Equivalent Circuit	39
III-1	Schematic of all Metal Vacuum System	46
III-2	The Plasma Package	48
III-3	Theoretical Phase Shift and Attenuation across 1-inch Plasma Slab Contained within 0.1 inch Glass Plates as Function of P	54
III-4	Voltage Current Characteristics for Hydrogen Discharge in Tube 5	57
III-5	Voltage Current Characteristic for Hydrogen Discharge	58
III-6	Ignition and Turn-off Voltages for Hydrogen Discharge	59
III-7	Normalized Plasma Frequency as Function of Hydrogen Discharge in Tube 4. Pressure = 0.1 Torr	61

LIST OF ILLUSTRATIONS (cont'd)

III-8	Normalized Plasma Frequency as Function of Hydrogen Discharge Current in Tube 4. Pressure = 0.23 Torr	62
III-9	Normalized Plasma Frequency as Function of Hydrogen Discharge Current in Tube 4. Pressure = 0.4 Torr	63
III-10	Normalized Plasma Frequency in Hydrogen Discharge as Function of Discharge Current at 0.4 Torr and Position of Receiving Horn for Tube 4.	64
III-11	Normalized Plasma Frequency as Function of Hydrogen Discharge Current in Tube 4. Pressure = 0.8 Torr	65
III-12	Voltage Current Characteristics for Xenon Discharge in Tube 4.	67
III-13	Ignition and Turn-off Voltages for Xenon Discharge in Tube 4.	68
III-14	Normalized Plasma Frequency as Function of Xenon Discharge Current in Tube 4. Pressure = 0.25 Torr	70
III-15	Normalized Plasma Frequency as Function of Xenon Discharge Current in Tube 4. Pressure = 0.5 Torr	71
III-16	Normalized Plasma Frequency as Function of Xenon Discharge Current in Tube 4. Pressure = 1.17 Torr	72
III-17	Modulation of Transmitted RF Power and Discharge Current by Plasma Oscillation in Xenon Gas at 0.4 Torr	75

EVALUATION

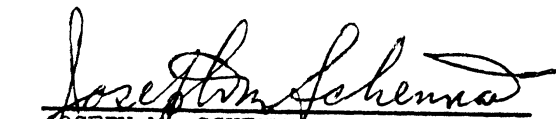
This program has been concerned with a theoretical and experimental investigation of microwave structures containing a plasma under the influence of a variable applied dc magnetic field and to determining the feasibility of developing practical microwave devices from such structures. Reciprocal and nonreciprocal propagation of electromagnetic waves in an ionized gaseous media and the ability to control and understand the intrinsic properties of the media and its anisotropic behavior under the influence of an applied magnetic field were some of the areas of interest.

In this phase of the study considerable attention was given to a plasma resonance isolator and to the design and fabrication of an improved plasma package (envelope) specifically intended for microwave applications. First order theory for calculating the absorption characteristics of the plasma resonance isolator was developed and compared with some experimental data. A theoretical tensor permittivity model and an equivalent scalar permittivity model were developed to describe the plasma-electromagnetic interaction and were found to produce similar results for the range of values and variables investigated. Good approximations to the actual absorption in the magneto-ionic medium were obtained when the operating microwave frequency is close to the electron cyclotron frequency and the electron collision frequency is assumed small. In addition to the anticipated cyclotron resonance absorption, a strong isolation was obtained by a nonreciprocal mode conversion in the plasma medium; i.e., energy in the fundamental TM_{11} mode is changed to a nonsymmetrical mode and is absorbed in the waveguide structure. It was further found that the absorption peaks associated with the mode conversion in the no-plasma condition were strongly enhanced under a magneto-plasma situation.

The experimental phase of this effort found that higher plasma frequencies are obtainable in hot discharges over that which can be obtained in cold discharges; that the plasma frequency of xenon discharges is 50 percent greater than hydrogen discharges at a fixed discharge current and pressure; that both media exhibited low frequency oscillations and that the oscillations observed in xenon were seen at all pressures, decreasing as the pressure increased.

Successful exploitation of plasmas in microwave devices is contingent upon obtaining a sufficiently stable plasma package that can be controlled in some desirable and useful manner. The principal plasma instabilities arise from plasma oscillations, gas cleanup and cathode deterioration; the second being the most serious contributor. Solution to the instability problems could result in microwave devices comparable to or better than conventional components and could lead to new and novel microwave circuits applicable to surveillance technology. This program has contributed valuable experience and knowledge to the scientific community and to those

graduate students engaged in this investigation. This program has further shown that a continuous effort in the area of basic and applied research is necessary to a better understanding and utilization of the intrinsic phenomena in plasmas.


JOSEPH M. SCHENNA
Project Engineer
RADC, GAFB, NY

I INTRODUCTION

This investigation has been concerned with the application of plasmas in microwave circuits with or without the presence of static magnetic fields. The elementary properties of plasmas and the characteristics of plasma devices that have been successful are first reviewed. Some of the areas where future advances in plasma applications can be expected are indicated.

The simplest type of electrical plasmas is a mixture of three phases: neutrals, ions and electrons. To a first order each phase may be specified by density (i. e. the number of particles per unit volume) and temperature (i. e. a characterization of the kinetic energy content of the phase on a per unit value basis at every point). The electrostatic forces of electrons and ions insure that, on a scale larger than the Debye shielding distance, the plasma is charge-density-wise neutral, i. e. electron and ion densities are equal. The ions, being from three to four orders of magnitude heavier than the electrons, respond that much less to the applied electric field and therefore they may be regarded as a stationary positive charge density distribution in which the electrons move.

In radio and microwave engineering plasmas the electron density and hence, also the ion density, is usually one per cent or less of the neutral molecule density. The temperature of the neutral molecules is of the same order of magnitude as the plasma container walls in those cases where the plasma chamber dimensions are not very many times the mean-free-path length of the neutral molecules. The temperature of the ions is somewhat higher than that of the neutrals. But, the temperature differences are not large owing to the fact that the neutral and the ion phases are rather closely coupled through equal collision cross sections and the two types of particles have essentially the same mass. The electron temperature is considerably higher than that of the ions or the neutrals. The temperature difference

is dependent on the type of gas used, and the method of exciting the plasma.

There are two ways of exciting a plasma: thermal excitation and electrical excitation. In a sealed envelope where one has to keep the surfaces from deteriorating, the range of temperatures to which one can heat the neutral gas is drastically limited. No significant volume ionization can be obtained even from cesium vapor, which has seen considerable use because single ionizations require only 3.87 electron volts. The ionization, however, is accomplished on the heater surface, the so-called 'contact ionization'. The heater is constantly under neutral cesium molecule bombardment; some of them remain long enough under the direct influence of the heater surface that they may be thought to be in thermal equilibrium with the latter and behaving as solid cesium in the electron emission properties. The work function of solid cesium is only about 1.81 eV, and thus it is clear that a considerable fraction of neutral cesium bombarding the hot heater surface (which in most cases is of tungsten) becomes ionized in the process. The ionized molecules then diffuse throughout the plasma volume. The electron-ion recombination in the volume and in the plasma sheath stabilizes the electron concentration for some particular gradient fitting the plasma volume. At the moment of ionization, the ions and the electrons have equal temperatures, both being close to the heater temperature (that is from 2000^o to 3000^oC) . After ionization, the ions are expected to give up the excess thermal energy to the local neutrals. As they diffuse away from the cathode, the electron gas however, having a weaker coupling with the neutrals than the ions, will relax at a slower rate and thus may be expected to have locally the highest temperature of the three phases.

We briefly summarize the desirable and undesirable properties of a plasma of this type. High electron densities may be achieved. The electron gas is of relatively low temperature and hence quiet electrically. Some instabilities may result

from the electron density gradients in the plasma volume, especially in the plasma sheath, and this will give rise to a semi-coherent frequency spectrum whose radiated energy is considerably above the thermal electron radiation. The vapors that may be ionized by 'contact' ionization are strongly active chemically and thus will attack glass to metal seals. Typical of these is cesium which, at standard temperature and pressure, has a melting point of 28.5°C and a boiling point of 670°C . The atoms which become lodged in the electrodes or the container walls may be replaced from a convenient pool of cesium in the plasma. A disadvantage is that diffusion of cesium into the walls of the container will make it electrically conducting, and hence lossy to microwaves. Also the density of cesium atoms will depend on the temperature of the plasma container walls. The electron density is determined by both the heater temperature and the cesium gas density.

Electrical excitation of plasmas is accomplished primarily in noble gases. Either cold or hot cathode discharge may be employed. The neutral molecules, the ions, and the plasma container walls all have temperatures of the same order of magnitude, whereas the electron temperature is higher by two to three orders of magnitude. The electrons, because of the large charge to mass ratio, are strongly coupled to the electric field causing the discharge and hence they are the primary plasma agents for receiving energy from the source field. If there is a sufficient density of neutral molecules, the electrons, excluding the plasma sheath, then have essentially Maxwellian velocity distribution in the plasma proper. The high energy tail of the electron velocity distributions causes sufficient ionization of the neutrals to replace losses of local recombination of ions as well as diffusion loss of ions to the walls. Thermal radiation of electrons is considerably higher than in thermally excited plasmas, and plasma oscillations under certain conditions may be more pronounced than in the case first considered. The application of larger and larger electrostatic fields causes the electrons to become more and

more uncoupled from the other phases of the plasma and the so-called electron run-away occurs. When noble gases are used for the discharge, one is required to start with a fixed density and no convenient mass reservoir is possible to provide replacement of the gas lost to the container walls and electrodes. This results in a decreasing gas density as the discharge progresses and the phenomena is referred to as gas cleanup. Mercury vapor may be used (melting point -38.87°C and boiling point 356.9°C at S.T.P) by including a drop of mercury in the envelope, but then as in the case of cesium, the vapor density, to a first order, would depend on the container wall temperature.

Present Uses for Plasmas

We have briefly reviewed the dependence of the basic plasma properties on the method of producing the plasma and the classes of gases employed. Now we wish to discuss present uses of plasmas and additional uses in the present day technology, some of which have already been attempted.

Electrostatic Voltage References and Voltage Regulators

Use is made of the fact that in the production of glow discharge plasma electron emission from cold metal surfaces under the action of ion bombardment occurs at characteristic ion energies. This is typically between 100 and 1000 volts and for a given noble gas and metal combination, to first order, is independent of gas pressure and the cold cathode temperature variations that occur in application environments. The gas cleanup which occurs in a device of this type is tolerable because a reserve capacity in the cathode area may be easily provided to accommodate currents that are demanded from the tube.

Noise Source for Microwave Receiver Calibration

This application arises from the fact that plasma electrons may be heated to high temperatures by electrostatic fields and therefore in the microwave range of

frequencies the non-coherent electromagnetic radiation from the electrons has a constant spectral density. As the gas density is decreased because of cleanup the properties of the electron noise radiation field also change, but this may be controlled by the discharge current, within limits.

TR Switches for Radar Receiver Protection

The operation of the device depends on the fact that a highly ionized gas is a good conductor, and when placed across a waveguide it reflects any incident microwave power. These devices may be pre-fired with a dc voltage pulse employing cold cathode emission, or one may depend directly on the radar pulse breakdown. However, one then has to contend with leakage of microwave power until the ionization has progressed far enough to cut off the signal. One of the main problems is the progressive gas cleanup under high power operation which at the present time limits the useful life of the device. During its useful life, however, the device operates successfully because small decreases of conductivity are not important to its operation as long as the conductivity does not fall below a certain level. Again one uses a reserve capacity of the gas to keep the tube in operation.

Plasma as the Source of Ultraviolet Light for Excitation of Fluorescent Materials

In the present day technology fluorescent lighting is widely used and here a plasma plays a useful role as an intermediate excitation source. The gradual cleanup of the gas in the fluorescent light tubes eventually stops the tube from lighting up, but by designing a reserve capacity in the tube, one can nevertheless obtain economic operation.

Hot Cathode Gas Filled Triodes (Thyratrons) for Switching Low Frequency Power

In these devices the conductivity of the plasma is used effectively to accomplish the switching function and the progressive gas cleanup may be tolerated, up

to a point. Alternatively one may use a drop of mercury as a source to replenish the molecules that are lost from the volume.

Plasma Masers

Plasma is a medium in which the free electron phase under most conditions has essentially a Maxwellian velocity distribution. This constitutes a broad exciting force. The electrons, by colliding with the neutrals, may excite nearly every state possible in the atoms. This state of affairs may be enhanced to some advantage by a judicious mixture of gases. Thus, a mixture of helium and neon produces a plasma in which a certain excited state of neon has a much larger population than in thermal equilibrium as a result of neon atoms colliding with helium atoms excited in the metastable state. If this plasma is placed in a resonant electromagnetic cavity and the cavity is tuned such that one of its resonant frequencies corresponds to an appropriate transition energy of the excited neon atoms, then the resonant electromagnetic cavity field will force the transitions to occur in an ordered manner phase-wise, and space and time coherent fields will grow in the cavity. This phenomena is known as stimulated emission and the mechanism has been successfully used in the design of masers for high infrared, and light frequencies. Since plasma excitation is not extreme and pressures are reasonable the gas cleanup problem is not severe.

Possible Plasma Applications

We have very briefly reviewed some successful plasma applications. The frequency spectrum coverage is wide indeed: from zero frequency up to and including light frequencies. However, a large gap exists in this coverage. All these applications are successful because they make demands on the plasma that are consistent with the nature of the plasma. These applications, so to speak, take into

account the fact that plasma is continuously changing, because it is reacting with the plasma container walls, as well as with electrodes which may be present. The gas cleanup problem is not severe because either the levels of gas density and ionizing force insure this, or an excess capability is designed into the device. Furthermore, in all cases the key mechanism (or parameter) for the operation of the device is completely independent of the changing character of the plasma, or sufficiently weakly dependent on it so that this is tolerable. Attempts which have been made to extend the application of plasmas beyond these limitations have not been sufficiently successful to be competitive with alternate approaches of design available.

In the light of these observations we have to ask ourselves which areas hold promise of some further potential application. One of the key limitations of the application of plasmas in microwaves, as has been recognized by a number of people, is the gas cleanup problem. Very little has been done so far either to understand it, or to design the plasma package in such a way as to minimize the process. Some questions which must be answered are:

What is the cleanup mechanism in a high power microwave discharge?

Is it accomplished by the electrons or ions?

Do they pick up the energy from the field in the body of the plasma, or in the plasma sheath?

What is the influence of the mean free path of ions and electrons as compared with the dimensions of the plasma passage?

To what extent do the cathode and other electrodes that are intended to maintain the plasma contribute to the gas cleanup by sputtering?

Is a ceramic plasma envelope superior to a glass envelope from the gas cleanup standpoint?

Work is in progress at the Microwave Associates on some of these problems (Maddix, et al, 1962, 1963). The problem is difficult and it has many ramifications. Most probably it cannot be eliminated, but hopefully, it can be reduced to tolerable levels.

It is very doubtful if any application of plasma in microwave circuits can be devised that depends critically on the constancy of plasma frequency as a function of time. The gas cleanup, temperature changes, and other processes in the plasma package will insure that plasma frequency will have a complicated behavior as a function of time under most conditions of operation.

One potential advantage of a plasma is that its properties can be varied by changing the electrical excitation force. Thermal plasmas can be varied by changing the heater current, perhaps the maximum rate is of the order of 1 Kc. Discharge plasmas have a higher rate of variation possible since the relaxation mechanisms are faster. The time interval necessary to ionize a gas is of the order of 1 microsecond. The plasma will return to a neutral state in the same time interval. These are the natural rates that are come by easily. Using large electric fields one may be able to speed up the ionization process; however, the reverse process cannot be made to go faster and this is a basic limitation. Since the ionizing agency is the main tool for changing the plasma properties it is clear that it is very difficult to change them in a prescribed and well-repeatable manner. However, there may be applications where this is tolerable. In any case, the on-off property of plasma may be used as a switch. However, faster switching rates than 1 Mc are in demand and not so easily obtained.

There is a big frequency interval from sub-millimeter waves up to medium infrared for which we do not have a coherent source. Attempts to decrease this frequency gap are being made from both ends. However, the suggested methods such as frequency multiplication, difference frequency methods, and megavolt beam electronics appear as brute force approaches and therefore inherently not well suited. It would ~~indeed~~ be amazing if nature did not possess a mechanism particularly tailored for this frequency interval. It is highly probable that plasma which is a highly excited state of matter may offer such a mechanism. Unfortunately

on the basis of present knowledge we cannot as yet propose a promising approach.

No application heretofore has been found for the cyclotron frequency of either the electron or ion, a parameter which is specified by the external magnetic field and, as such, is invariant for a changing plasma. The reason for this is that in attempted applications such as microwave phase shifting, the cyclotron frequency acts together with the plasma frequency and the collision frequency. Both latter parameters are very sensitive functions of plasma excitation force and gas density, respectively. Therefore, the plasma phase shifter is erratic in its performance. On the other hand, the cyclotron frequency determines the center frequency of the resonance isolator. The plasma frequency and the collision frequency determine the width and height of the absorption peak. Some changes may be tolerated in this without seriously impairing the usefulness of the device.

The goal of the present investigation was the development of a suitable and convenient plasma package for utilization in microwave circuitry. A specific application in the microwave area is the isolator, a non-reciprocal device using the interaction of guided waves with a magneto-plasma, thus incorporating the electron cyclotron resonance phenomena in a useful component. A theoretical study concerning the isolator was to be carried out and the compatibility of the experimental and theoretical results was to be examined.

THEORETICAL DERIVATION OF ABSORPTION IN THE ELECTRON CYCLOTRON RESONANCE ISOLATOR AND ITS EQUIVALENT CIRCUIT

We wish to compute the power transmission coefficient through a plasma cyclotron resonance isolator. The pertinent dimensions of the isolator and the coordinate system are shown in Fig. II-1. A TM_{11} mode propagates in the square cross section waveguide in the positive z -direction. A thin plasma slab in the bottom half of the waveguide extends from wall to wall in the x -direction. A magneto-static field is impressed on the plasma in the $+x$ - direction.

The power flow at each point in the z -direction, for any waveguide, may be characterized by an absorption coefficient α that is defined by (assuming propagation in the positive z -direction)

$$P(z) = P_{in} \exp \left[-2 \int_0^z \alpha(z') dz' \right], \quad (2.1)$$

where P_{in} is the input power, and $P(z)$ is the remaining power as the wave progresses in the guide. Differentiation of (2.1) yields

$$\alpha(z) = - \frac{1}{2P(z)} \frac{dP(z)}{dz} . \quad (2.2)$$

But since the time average of the divergence of the Poyntings vector, $\overline{\nabla \cdot \bar{S}}$, gives the negative density of the power absorbed in the medium we obtain,

$$\frac{dP(z)}{dz} = \iint_A \overline{\nabla \cdot \bar{S}} dx dy , \quad (2.3)$$

where A is the guide cross section. On substituting (2.3) in (2.2) we have

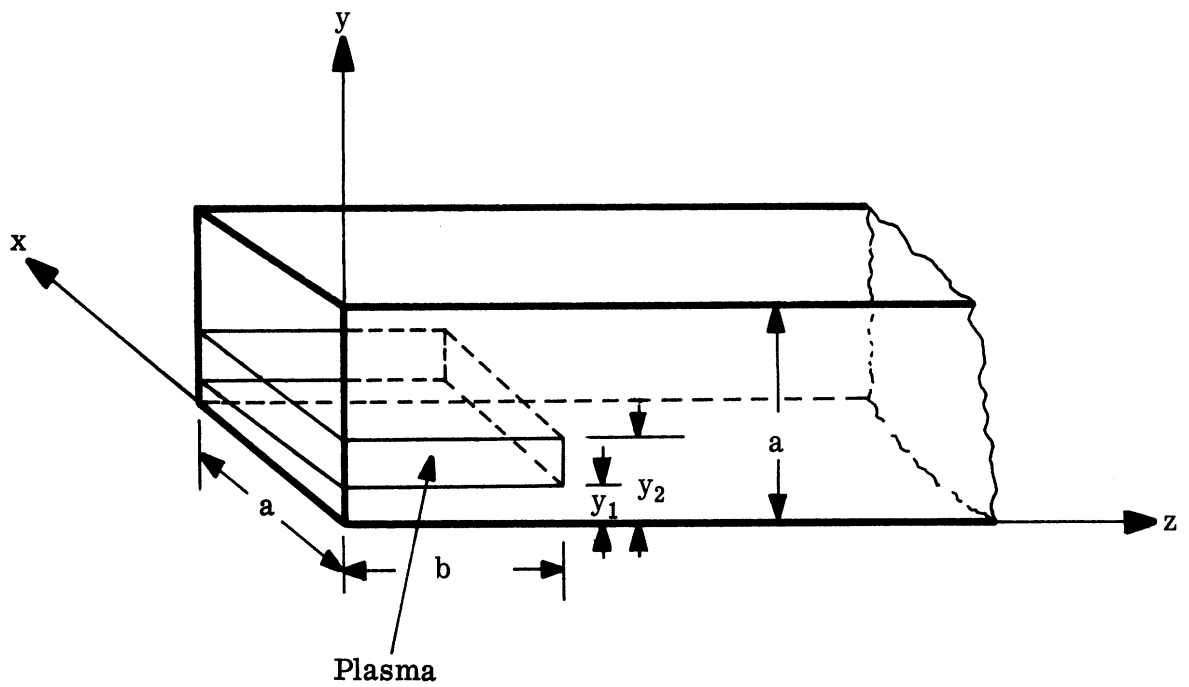


FIG. II-1: SKETCH OF ISOLATOR

$a=7.6$ cm, $b=7.7$ cm, $y_1=1.0$ cm, $y_2=2.5$ cm.

$$\alpha(z) = -\frac{1}{2P(z)} \int \int_A \overline{\nabla \cdot \vec{S}} \, dx \, dy \quad . \quad (2.4)$$

The power transmission coefficient (PTC) of the isolator is defined by

$$\text{PTC} \equiv 10 \log \frac{P_{\text{out}}}{P_{\text{in}}} \quad . \quad (2.5)$$

Neglecting the reflections from the ends of the isolator we have from (2.1) and (2.5)

$$\text{PTC} = -20 \log e \int_0^b \alpha(z') \, dz' \quad , \quad (2.6)$$

and since

$$P(z) = \frac{1}{2} \text{Re} \int \int_A \vec{E} \times \vec{H}^* \cdot \vec{a}_z \, dx \, dy \quad , \quad (2.7)$$

we have from (2.4) and (2.6) that

$$\text{PTC} = 20 \log e \int_0^b \left\{ \frac{\int \int_A \overline{\nabla \cdot \vec{S}} \, dx \, dy}{\text{Re} \int \int_A \vec{E} \times \vec{H}^* \cdot \vec{a}_z \, dx \, dy} \right\} dz \quad . \quad (2.8)$$

We see that in order to calculate the PTC one must have a model that describes the plasma-electromagnetic wave interaction so that the divergence of the power flow may be obtained.

The Tensor Model

The magneto-ionic plasma has a permittivity of the following form in our coordinate system:

$$\epsilon = \begin{bmatrix} \epsilon_{11} & 0 & 0 \\ 0 & \epsilon_{22} & \epsilon_{23} \\ 0 & \epsilon_{32} & \epsilon_{33} \end{bmatrix} . \quad (2.9)$$

The tensor elements are given by

$$\begin{aligned} \epsilon_{11} &= \epsilon_0 \left[1 + \frac{P^2}{j(V+j)} \right] , \\ \epsilon_{22} = \epsilon_{33} &= \epsilon_0 \left[1 + \frac{P^2(V+j)}{j(V+j)^2 + Y^2} \right] , \\ \epsilon_{23} = \epsilon_{32} &= \epsilon_0 \left[\frac{jYP^2}{(V+j)^2 + Y^2} \right] , \end{aligned} \quad (2.10)$$

where $P = \omega_P/\omega$, $V = \nu_c/\omega$, $Y = \omega_H/\omega$. ω_P , ω_H , and ω are the radian electron plasma frequency, electron cyclotron frequency and microwave frequency respectively. ν_c is the electron collision frequency. f_P , f_H and f , which appear later, are defined by $\omega_P = 2\pi f_P$, $\omega_H = 2\pi f_H$ and $\omega = 2\pi f$.

The time average divergence of Poyntings vector for an anisotropic dielectric is easily shown to be

$$\overline{\nabla \cdot \bar{S}} = -j \frac{\omega}{4} \left[\epsilon_{ik} - \epsilon_{ki}^* \right] E_i E_k^* . \quad (2.11)$$

In the above formula the tensor notation is used. Substituting (2.9) and (2.10) in (2.11) we have

$$\overline{\nabla \cdot \bar{S}} = -j \frac{\omega}{4} \left\{ (\epsilon_{11} - \epsilon_{11}^*) E_1^* E_1 + (\epsilon_{22} - \epsilon_{22}^*) (E_2^* E_2 + E_3^* E_3) + (\epsilon_{23} + \epsilon_{23}^*) (E_2^* E_3 - E_3^* E_2) \right\} , \quad (2.12a)$$

$$\epsilon_{11} - \epsilon_{11}^* = -2j\epsilon_0 \frac{VP^2}{1+V^2} \quad (2.12b)$$

$$\epsilon_{22} - \epsilon_{22}^* = -2j\epsilon_0 \frac{VP^2(Y^2+V^2+1)}{(Y^2+V^2-1)^2+(2V)^2} \quad (2.12c)$$

$$\epsilon_{23} + \epsilon_{23}^* = 4\epsilon_0 \frac{VP^2Y}{(Y^2+V^2-1)^2+(2V)^2} \quad (2.12d)$$

The isolator is operated normally in a state such that the following conditions on the parameters hold true:

$$V \ll 1 \quad , \quad (2.13a)$$

and

$$Y = 1 + \Delta Y \quad , \quad |\Delta Y| \ll 1 \quad . \quad (2.13b)$$

The condition (2.13a) implies that the first term on the right-hand side of (2.12a) is negligible compared to the remaining two terms. Thus further we consider

$$\overline{\nabla \cdot \bar{S}} \cong -j \frac{\omega}{4} \left\{ (\epsilon_{22} - \epsilon_{22}^*)(E_2^* E_2 + E_3^* E_3) + (\epsilon_{23} + \epsilon_{23}^*)(E_2^* E_3 - E_3^* E_2) \right\} \quad (2.14)$$

A special case of considerable interest is when the electric field in a plane normal to the magnetostatic field is circularly polarized. Then

$$E_3 = +j E_2 \quad (2.15)$$

and

$$\overline{\nabla \cdot \bar{S}} \cong -\epsilon_0 \frac{\omega}{2} VP^2 \frac{(Y+1)^2+V^2}{(V^2+Y^2-1)^2+(2V)^2} |E|^2 \quad (2.16)$$

where

$$|E|^2 = 2 |E_2|^2 = 2 |E_3|^2$$

and the \mp signs are correlated with the signs in (2.15). Applying conditions (2.13) to (2.16) and taking the leading terms we have in the case of the (-) sign

$$\overline{\nabla \cdot \bar{\mathbf{S}}}_{(-)} \simeq -\epsilon_0 \frac{\omega}{2} VP^2 \frac{1}{4} |\mathbf{E}|^2, \quad (2.17)$$

and in the case of the (+) sign

$$\overline{\nabla \cdot \bar{\mathbf{S}}}_{(+)} \simeq -\epsilon_0 \frac{\omega}{2} VP^2 \frac{1}{(\nabla Y)^2 + V^2} |\mathbf{E}|^2. \quad (2.18)$$

Equations (2.17) and (2.18) show that the time average divergence in the vicinity of the cyclotron resonance very strongly depends on the sense of the circular polarization of the electric field in the plane normal to the magnetostatic field. This is due to the fact that the sense of rotation of the electrons in a plane normal to the magnetostatic field is fixed, and in the case of (2.18) the electric field is rotating in the same sense whereas in (2.17), the electric field is rotating in the opposite sense to the natural direction of the electron rotation. Hence we have the striking difference in the time average of the Poyntings vector divergence.

The Equivalent Scalar Model

For the moment we leave this path of reasoning and consider the following. The time average divergence of the Poyntings vector in isotropic medium that has only dielectric losses may be written as

$$\overline{\nabla \cdot \bar{\mathbf{S}}} = -\frac{\omega}{2} \epsilon'' \bar{\mathbf{E}} \cdot \bar{\mathbf{E}}^* \quad (2.19)$$

where $\epsilon = \epsilon' - j \epsilon''$ is the permittivity of the medium and clearly is a scalar constant. However, also in the special case of a circularly polarized plane wave that is propagating along the magnetostatic field lines, the electrical flux density is related to the electric field by a scalar constant; an equivalent permittivity so to speak. We distinguish two waves: ordinary and extraordinary, depending on the sense of

polarization of the electric field. For the extraordinary wave the sense of polarization of the electric field is the same as the direction of rotation of electrons in the magnetostatic field, while for the ordinary wave it is opposite. One may be tempted to believe that it is permissible to take the imaginary parts of these equivalent permittivities and substitute them in (2.19). Then we obtain that in the case of the extraordinary wave

$$\overline{\nabla \cdot \bar{S}}_{\text{ex}} = -\epsilon_0 \frac{\omega}{2} VP^2 \frac{1}{(Y-1)^2 + V^2} \bar{E} \cdot \bar{E}^* \quad (2.20)$$

and in the case of ordinary wave

$$\overline{\nabla \cdot \bar{S}}_{\text{ord}} = -\epsilon_0 \frac{\omega}{2} VP^2 \frac{1}{(Y+1)^2 + V^2} \bar{E} \cdot \bar{E}^* . \quad (2.21)$$

The absorption for the ordinary wave should correspond to (2.16) with the (-) sign while the same equation with the (+) sign would apply to the extraordinary wave. Equation (2.16), however, does not reduce any further, and we have to conclude that (2.20) and (2.21) in general are not correct. But we are not interested in the total domain of the variables. Our concern is circumscribed by conditions (2.13). When we apply conditions (2.13) to (2.20) and (2.21) we have respectively:

$$\overline{\nabla \cdot \bar{S}}_{\text{ex}} \simeq -\epsilon_0 \frac{\omega}{2} VP^2 \frac{1}{(\nabla Y)^2 + V^2} \bar{E} \cdot \bar{E}^* , \quad (2.22)$$

and

$$\overline{\nabla \cdot \bar{S}}_{\text{ord}} \simeq -\epsilon_0 \frac{\omega}{2} VP^2 \frac{1}{4} \bar{E} \cdot \bar{E}^* . \quad (2.23)$$

It is clear that (2.22) corresponds to (2.18) and (2.23) corresponds to (2.17). We may conclude that (2.20) and (2.21) are good approximations to the actual absorption in the magneto-ionic medium in the case when the microwave frequency is close to the electron cyclotron frequency and the electron collision frequency is small

compared to the first. With these approximations in mind we will be using (2.20) and (2.21) in the first set of calculations. To shorten the notation we introduce the following.

$$\epsilon'_+ = \epsilon_0 VP^2 \frac{1}{(Y-1)^2 + V^2} \quad , \quad (2.24)$$

and

$$\epsilon'_- = \epsilon_0 VP^2 \frac{1}{(Y+1)^2 + V^2} \quad . \quad (2.25)$$

Isolator Absorption Formulae

Before we can proceed with the calculation of the power transmission coefficient we have to write down the form of the fields in the isolator. We consider the fields of the TM_{11} mode propagating in the positive z -direction in an empty guide. Within an arbitrary constant and assuming $e^{j\omega t}$ time dependence, they are (Ramo, Whinnery, 1960)

$$\begin{aligned} \bar{E} = & \left[-j\beta_{11} a \cos \frac{\pi x}{a} \sin \frac{\pi y}{a} \bar{a}_x - j\beta_{11} a \sin \frac{\pi x}{a} \cos \frac{\pi y}{a} \bar{a}_y \right. \\ & \left. + 2\pi \sin \frac{\pi x}{a} \sin \frac{\pi y}{a} \bar{a}_z \right] e^{-j\beta_{11} z} \quad , \quad (2.26) \end{aligned}$$

$$\bar{H} = j\omega \epsilon_0 a \left[\sin \frac{\pi x}{a} \cos \frac{\pi y}{a} \bar{a}_x - \cos \frac{\pi x}{a} \sin \frac{\pi y}{a} \bar{a}_y \right] e^{-j\beta_{11} z} \quad (2.27)$$

where

$$\beta_{11} = \sqrt{\omega^2 \mu_0 \epsilon_0 - 2 \left(\frac{\pi}{a} \right)^2} \quad .$$

In the context of using (2.20) and (2.21) we neglect E_x and hence we have

$$\bar{E} \cdot \bar{E}^* = a^2 \beta_{11}^2 \cos^2 \frac{\pi y}{a} \sin^2 \frac{\pi x}{a} + 4\pi^2 \sin^2 \frac{\pi x}{a} \sin^2 \frac{\pi y}{a} \quad . \quad (2.28)$$

Furthermore we have that

$$\text{Re} \int_A \bar{E} \times \bar{H}^* \cdot \bar{a}_z dx dy = \frac{1}{2} \omega \epsilon_0 \beta_{11} a^4 \quad . \quad (2.29)$$

We observe that introducing (2.24) and (2.28) in (2.22) we have

$$\overline{\nabla \cdot \bar{S}}_{\text{ex}} = -\frac{\omega}{2} \epsilon_+'' \left[a^2 \beta_{11}^2 \sin^2 \frac{\pi X}{a} \cos^2 \frac{\pi Y}{a} + 4\pi^2 \sin^2 \frac{\pi X}{a} \sin^2 \frac{\pi Y}{a} \right] \quad (2.30)$$

Substituting (2.29) and (2.30) in (2.8) we have

$$\begin{aligned} \text{PTC} \simeq -20 \log e \int_0^b dz \int_{y_1}^{y_2} dy \int_0^a dx \left[\frac{\beta_{11}}{a^2} \sin^2 \frac{\pi X}{a} \cos^2 \frac{\pi Y}{a} \right. \\ \left. + \frac{4\pi^2}{\beta_{11} a^4} \sin^2 \frac{\pi X}{a} \sin^2 \frac{\pi Y}{a} \right] \frac{\epsilon_+''}{\epsilon_0} \quad . \quad (2.31) \end{aligned}$$

When ϵ_+'' in the preceding equation is independent of coordinates, we may integrate the above expression to

$$\begin{aligned} \text{PTC} \simeq \frac{-5b \log e}{\beta_{11}} \left\{ \frac{y_2 - y_1}{a} \left[\beta_{11}^2 + \left(\frac{2\pi}{a} \right)^2 \right] + \right. \\ \left. \frac{1}{2\pi} \left(\sin \frac{2\pi y_2}{a} - \sin \frac{2\pi y_1}{a} \right) \left[\beta_{11}^2 - \left(\frac{2\pi}{a} \right)^2 \right] \right\} \frac{VP^2}{(Y-1)^2 + V^2} \quad . \quad (2.32) \end{aligned}$$

Using (2.24) and the dimensions of Fig. II-1 for a frequency of 3.9 Gc, the equation (2.32) reduces to

$$\text{PTC} \simeq -5.6 \frac{P^2 V}{(Y-1)^2 + V^2} \quad . \quad (2.33)$$

In Fig. II-2 the PTC of (2.33) is plotted as a function of Y for $V = 0.0327$ and $P = 0.256$. We observe a sharp resonance at $Y=1$, i. e. $\omega = \omega_H$.

Measurements on the magnetostatic field show that the field at the center of the plasma chamber is about 15 per cent less than at the edges. Since ϵ_+'' is

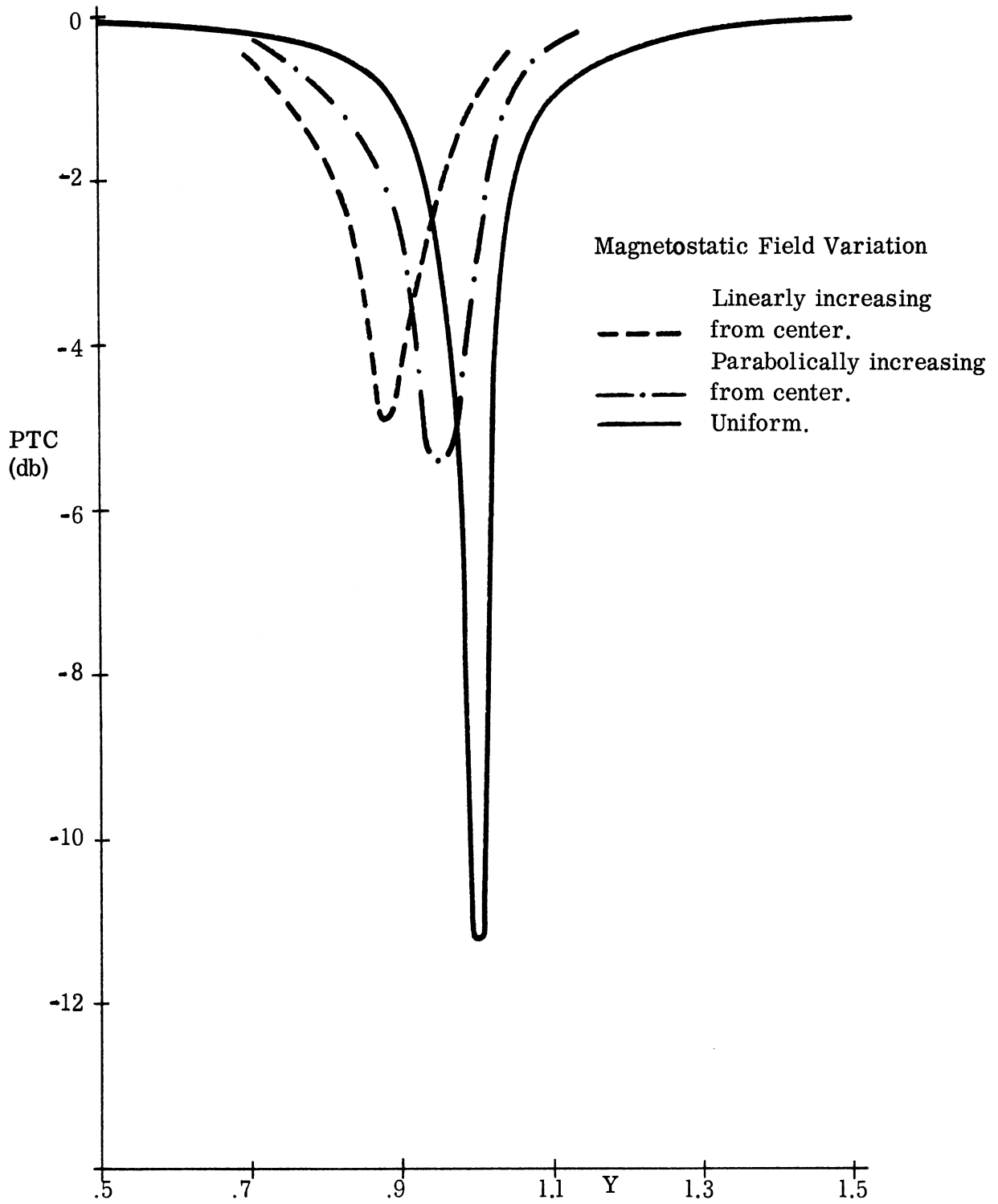


FIG. II-2: POWER TRANSMISSION COEFFICIENT AS FUNCTION OF Y CALCULATED FROM EXTRAORDINARY WAVE APPROXIMATION EQN (2.33). $f = 3.9$ Gc, $f_p = 1.0$ Gc, $\nu_c = 0.8$ Gc, $Y = \omega_H/\omega$

dependent upon the cyclotron frequency and hence on the magneto-static field strength, it follows that (2.32) is not strictly applicable in our case. In order to determine the effect upon the PTC of a non-uniform magneto-static field, the integration of (2.31) was performed for the cases of parabolic and linear increase of the magneto-static field in the x- and z-directions from the center of the plasma volume. Since the extent of the plasma in the y-direction is rather small compared to the waveguide size, the magneto-static field in this coordinate was assumed constant. The integration was performed numerically, using, as before, a microwave frequency of 3.9 Gc, a collision frequency of 0.8 Gc, and a plasma frequency of 1 Gc. In Fig. II-2 we have shown the above calculations. We notice that the resonance absorption peaks are considerably broadened, very much reduced in amplitude and shifted to the left as compared to the constant magneto-static field case. The magneto-static field at the center of the plasma is the same as in the uniform case, but it is assumed higher around the rim of the plasma package. This gives rise to the effects shown.

At this point we should summarize the approximations which have not been pointed out explicitly in the calculation of the graphs of Fig. II-2.

(1) The field in the plasma has the same transverse variation as in the empty guide and there is no reflected wave in the plasma section of the guide. This assumption will also be used in subsequent calculations.

(2) The longitudinal electric field of the TM_{11} mode is not circularly polarized throughout the plasma cross section, but we are proceeding as if it were.

(3) The magneto-ionic plasma slab does not convert energy from the TM_{11} mode into the TE_{10} or TE_{01} mode which are also propagating modes in our square waveguide.

(4) The presence of the glass envelope enclosing the plasma is ignored.

When the direction of propagation of the TM_{11} mode is reversed, i. e. it is propagating in the negative z -direction, then the PTC may be computed from (2.31) by substituting for ϵ_+'' the imaginary part of the equivalent permittivity for the ordinary wave, ϵ_-'' given by (2.25). This loss is negligible for $V \ll 1$ and $Y \sim 1$; our region of interest.

In the preceding discussion it was assumed that the longitudinal field of the TM_{11} mode was circularly polarized throughout the plasma slab. The assumption holds only for the center plane of the slab. For the rest, the field is elliptically polarized. We may remove this approximation, if we decompose the elliptically polarized electric field into two oppositely rotating, unequal amplitude, circularly polarized fields. We thus let

$$\vec{E} = \left[\vec{A}_+ + \vec{B}_- \right] e^{-j\beta_{11}z}, \quad (2.34)$$

with

$$\vec{A}_+ = A_2 \left[\vec{a}_y + j \vec{a}_z \right] \quad (2.35a)$$

$$\vec{B}_- = B_2 \left[\vec{a}_y - j \vec{a}_z \right] \quad (2.35b)$$

where

$$A_2 = -\frac{1}{2} j \sin \frac{\pi X}{a} \left[a \beta_{11} \cos \frac{\pi Y}{a} + 2\pi \sin \frac{\pi Y}{a} \right] \quad (2.36a)$$

$$B_2 = -\frac{1}{2} j \sin \frac{\pi X}{a} \left[a \beta_{11} \cos \frac{\pi Y}{a} - 2\pi \sin \frac{\pi Y}{a} \right]. \quad (2.36b)$$

The time average divergence of Poyntings vector from (2.19) is

$$\overline{\nabla \cdot \vec{S}} \cong -\frac{\omega}{2} \left[\epsilon_+'' \vec{A}_+ \cdot \vec{A}_+^* + \epsilon_-'' \vec{B}_- \cdot \vec{B}_-^* \right] \quad (2.37)$$

It would appear that we are mis-using superposition to obtain the above formula. In fact, we are not using that principle in either sense. We may easily show that

the power absorption in the magneto-ionic medium does not couple for the ordinary and the extraordinary waves. We consider a medium that has only dielectric losses.

Then

$$\overline{\nabla \cdot \bar{S}} = -\overline{\bar{E} \cdot \frac{\partial \bar{D}}{\partial t}} \quad (2.38)$$

Considering two circularly polarized waves:

$$\bar{D}_1 = \epsilon_1 \bar{E}_1 ; \epsilon_1 = \epsilon'_1 - j \epsilon''_1 \quad (2.39a)$$

and

$$\bar{D}_2 = \epsilon_2 \bar{E}_2 ; \epsilon_2 = \epsilon'_2 - j \epsilon''_2 \quad , \quad (2.39b)$$

with

$$\bar{E}_1 = E_1 (\bar{a}_x + j \bar{a}_y) \quad (2.40a)$$

$$\bar{E}_2 = E_2 (\bar{a}_x - j \bar{a}_y) \quad . \quad (2.40b)$$

We introduce complex notation in (2.38) by letting

$$\bar{E} \rightarrow \frac{1}{2} (\bar{E}_1 + \bar{E}_1^*) + \frac{1}{2} (\bar{E}_2 + \bar{E}_2^*) \quad (2.41)$$

$$\frac{\partial \bar{D}}{\partial t} \rightarrow \frac{1}{2} (j\omega \epsilon_1 \bar{E}_1 - j\omega \epsilon_1^* \bar{E}_1^*) + \frac{1}{2} (j\omega \epsilon_2 \bar{E}_2 - j\omega \epsilon_2^* \bar{E}_2^*) \quad , \quad (2.42)$$

and substituting the two preceding equations in (2.38) we obtain

$$\overline{\nabla \cdot \bar{S}} = -\frac{\omega}{2} \left[\epsilon''_1 \bar{E}_1 \cdot \bar{E}_1^* + \epsilon''_2 \bar{E}_2 \cdot \bar{E}_2^* \right] - \frac{\omega}{2} \left[(\epsilon_2 - \epsilon_1^*) \bar{E}_1 \cdot \bar{E}_2 + (\epsilon_1 - \epsilon_2^*) \bar{E}_1 \cdot \bar{E}_2^* \right] . \quad (2.43)$$

Applying (2.40a) and (2.40b) in (2.43) we see that

$$\bar{E}_1^* \cdot \bar{E}_2 = E_1^* E_2 (\bar{a}_x - j \bar{a}_y) \cdot (\bar{a}_x - j \bar{a}_y) = 0 \quad , \quad (2.44)$$

$$\bar{E}_1 \cdot \bar{E}_2^* = E_1 E_2^* (\bar{a}_x + j \bar{a}_y) \cdot (\bar{a}_x + j \bar{a}_y) = 0 \quad , \quad (2.45)$$

and hence the second term vanishes in (2.43) and consequently we have established that (2.37) is valid, subject only to approximations discussed previously.

We return to the calculation of the power transmission coefficient. In (2.37) we may neglect the second term. Substituting the remainder in (2.8) in the same

sense as before we obtain:

$$\text{PTC} = -10 \log e \int_0^b dz \int_{y_1}^{y_2} dy \int_0^a dx \left\{ \frac{\epsilon''}{\epsilon_0} \sin^2 \frac{\pi x}{a} \right. \\ \left. \left[\frac{4\pi^2}{\beta_{11} a^4} \sin^2 \frac{\pi y}{a} + \frac{\beta_{11}}{a^2} \cos^2 \frac{\pi y}{a} + \frac{4\pi}{a^3} \sin \frac{\pi y}{a} \cos \frac{\pi y}{a} \right] \right\}. \quad (2.46)$$

For constant magnetostatic field we can integrate the above equation to

$$\text{PTC} \simeq \frac{-5b \log e}{\beta_{11}} \left\{ \frac{1}{2} \frac{[y_2 - y_1]}{a} \left[\beta_{11}^2 + \left(\frac{2\pi}{a}\right)^2 \right] \right. \\ + \frac{1}{4\pi} \left[\sin \left(\frac{2\pi y_2}{a}\right) - \sin \left(\frac{2\pi y_1}{a}\right) \right] \left[\beta_{11}^2 - \left(\frac{2\pi}{a}\right)^2 \right] \\ \left. + \frac{2\beta_{11}}{a} \left[\sin^2 \left(\frac{\pi y_2}{a}\right) - \sin^2 \left(\frac{\pi y_1}{a}\right) \right] \right\} \frac{VP^2}{(Y-1)^2 + V^2}. \quad (2.47)$$

The dependence on plasma parameters remains the same as in (2.32), however the first two terms in the brackets is exactly one-half of those corresponding in (2.32). The third term increases the result considerably, but it is linear in β_{11} and thus cannot compensate the β_{11}^2 term over a large frequency band exactly. This formula is 5 per cent less than (2.32) for the numerical case discussed in (2.33), and the disagreement increases to 14 per cent as the frequency goes to 3 Gc; the other parameters remaining the same. We conclude that when the plasma slab is not sufficiently thin or properly placed we should take into account the elliptical polarization.

We have shown that close to the gyromagnetic resonance and for small collision frequency the absorption of the electromagnetic energy by the plasma may be accounted for by an equivalent permittivity obtained from the extraordinary plane wave representation. We would like to know how far from the gyromagnetic resonance we may safely use this elementary model. Thus we want to compare (2.46) with that obtained from the tensor representation of the permittivity. Substituting (2.12) and (2.28) in (2.8) we have

$$\begin{aligned}
\text{PTC} \simeq j \frac{10 \log e}{\epsilon_0} \int_0^b dz \int_{y_1}^{y_2} dy \int_0^a dx \left\{ (\epsilon_{11} - \epsilon_{11}^*) \frac{\beta_{11}}{a^2} \cos^2 \frac{\pi x}{a} \sin^2 \frac{\pi y}{a} \right. \\
+ \sin^2 \frac{\pi x}{a} \left[(\epsilon_{22} - \epsilon_{22}^*) \left(\frac{\beta_{11}}{a^2} \cos^2 \frac{\pi y}{a} + \frac{4\pi^2}{\beta_{11} a^4} \sin^2 \frac{\pi y}{a} \right) \right. \\
\left. \left. - (\epsilon_{23} + \epsilon_{32}^*) \frac{j4\pi}{a^3} \cos \frac{\pi y}{a} \sin \frac{\pi y}{a} \right] \right\} . \quad (2.48)
\end{aligned}$$

After integration we obtain for constant magneto-static field

$$\begin{aligned}
\text{PTC} \simeq j \frac{5b \log e}{\beta_{11} \epsilon_0} \left\{ (\epsilon_{11} - \epsilon_{11}^*) \frac{\beta_{11}^2}{4\pi} \left(\frac{2\pi}{a} [y_2 - y_1] - \left[\sin \frac{2\pi y_2}{a} - \sin \frac{2\pi y_1}{a} \right] \right) \right. \\
+ (\epsilon_{22} - \epsilon_{22}^*) \left(\frac{1}{4\pi} \left[\beta_{11}^2 - \left(\frac{2\pi}{a} \right)^2 \right] \left[\sin \frac{2\pi y_2}{a} - \sin \frac{2\pi y_1}{a} \right] + \frac{1}{2a} \left[\beta_{11}^2 + \left(\frac{2\pi}{a} \right)^2 \right] [y_2 - y_1] \right) \\
\left. - \frac{2j\beta_{11}}{a} (\epsilon_{23} + \epsilon_{32}^*) \left(\sin^2 \frac{\pi y_2}{a} - \sin^2 \frac{\pi y_1}{a} \right) \right\} . \quad (2.49)
\end{aligned}$$

For the dimensions shown in Fig. II-1, and the assumption of small collision frequency, computation from (2.47) and (2.49) produced essentially the same results for $0.5 < Y < 1.5$, independent of P.

We further test the agreement for non-uniform static magnetic field. A magnetic field variation given by

$$Y = Y_0 \left[1 + \Delta Y_0 \left(\frac{2x}{a} - 1 \right)^2 \right] \left[1 + \Delta Y_0 \left(\frac{2z}{b} - 1 \right)^2 \right] , \quad (2.50)$$

is typical for the experimental situation where Y_0 represents the normalized electron cyclotron frequency at the center of the plasma and ΔY_0 is the fractional variation in the static magnetic field (and as a result, the variation in the electron cyclotron frequency) between center and edge of the plasma. No magnetic field variation was considered in the y-coordinate since this was the narrow dimension of the plasma slab and the field was quite uniform over this dimension. Numerical integration of (2.46) and (2.48) has been carried out. The results of these calculations are shown in Figs. II-3 through II-6. Figures II-3 and II-5, respectively, show the PTC for the equivalent scalar permittivity case when the microwave frequency is varied for a fixed magnetic field strength ($f_{HO} = 3.72$) and when the electron cyclotron frequency is varied for a fixed microwave frequency ($f = 3.90$ Gc). The corresponding results for the tensor permittivity case are shown in Figs. II-4 and II-6. ΔY_0 is increased from 0 in equal steps of 0.05. In these curves ν_c is 0.8 Gc and f_p is 1.0 Gc. The parameter values were chosen to agree with some experimental data. These curves are shown in continuous lines rather than marking each data point on the curve, for the sake of clarity. In other theoretical curves presented here, the data points will be shown. Note that the PTC in db for any plasma frequency may be obtained from these results by multiplying by the square of the plasma frequency expressed in Gc.

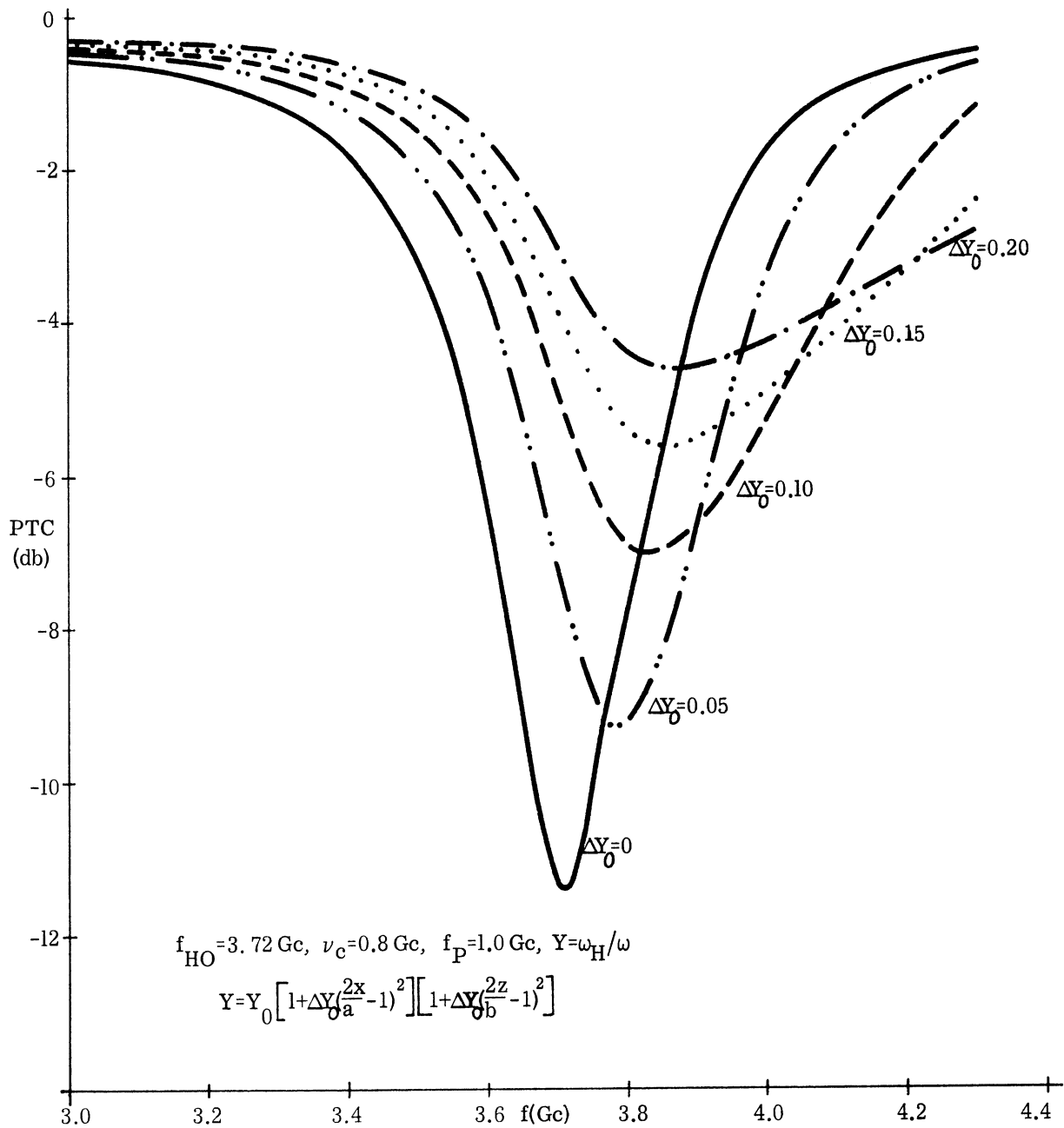


FIG. II-3: POWER TRANSMISSION COEFFICIENT AS FUNCTION OF FREQUENCY
 CALCULATED FROM EXTRAORDINARY WAVE APPROXIMATION WITH
 ELLIPTICAL POLARIZATION ACCOUNTED FOR AND PARABOLIC
 MAGNETIC FIELD VARIATION

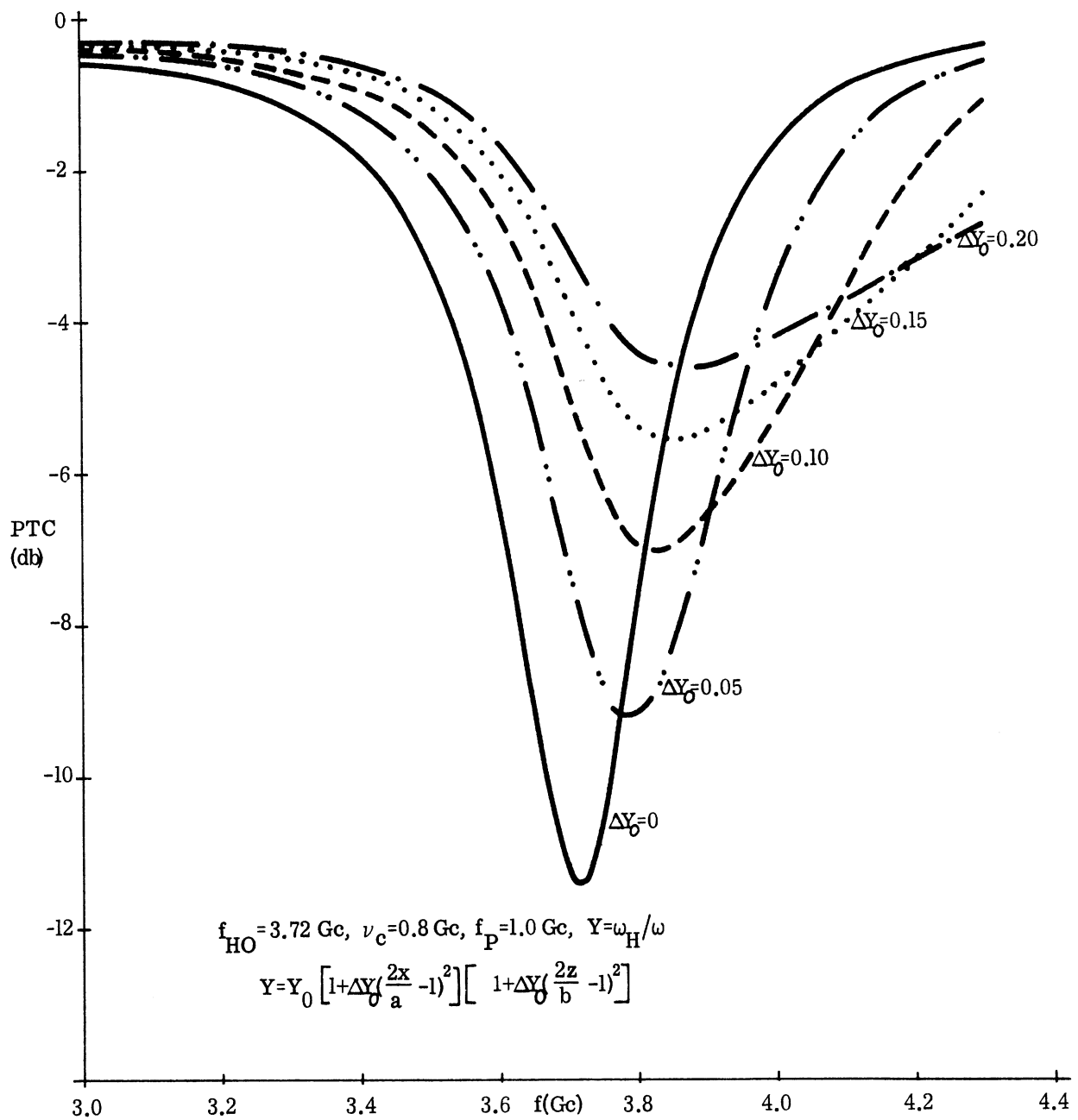


FIG II-4: POWER TRANSMISSION COEFFICIENT AS FUNCTION OF FREQUENCY CALCULATED FOR TENSOR PERMITTIVITY AND PARABOLIC MAGNETIC FIELD VARIATION

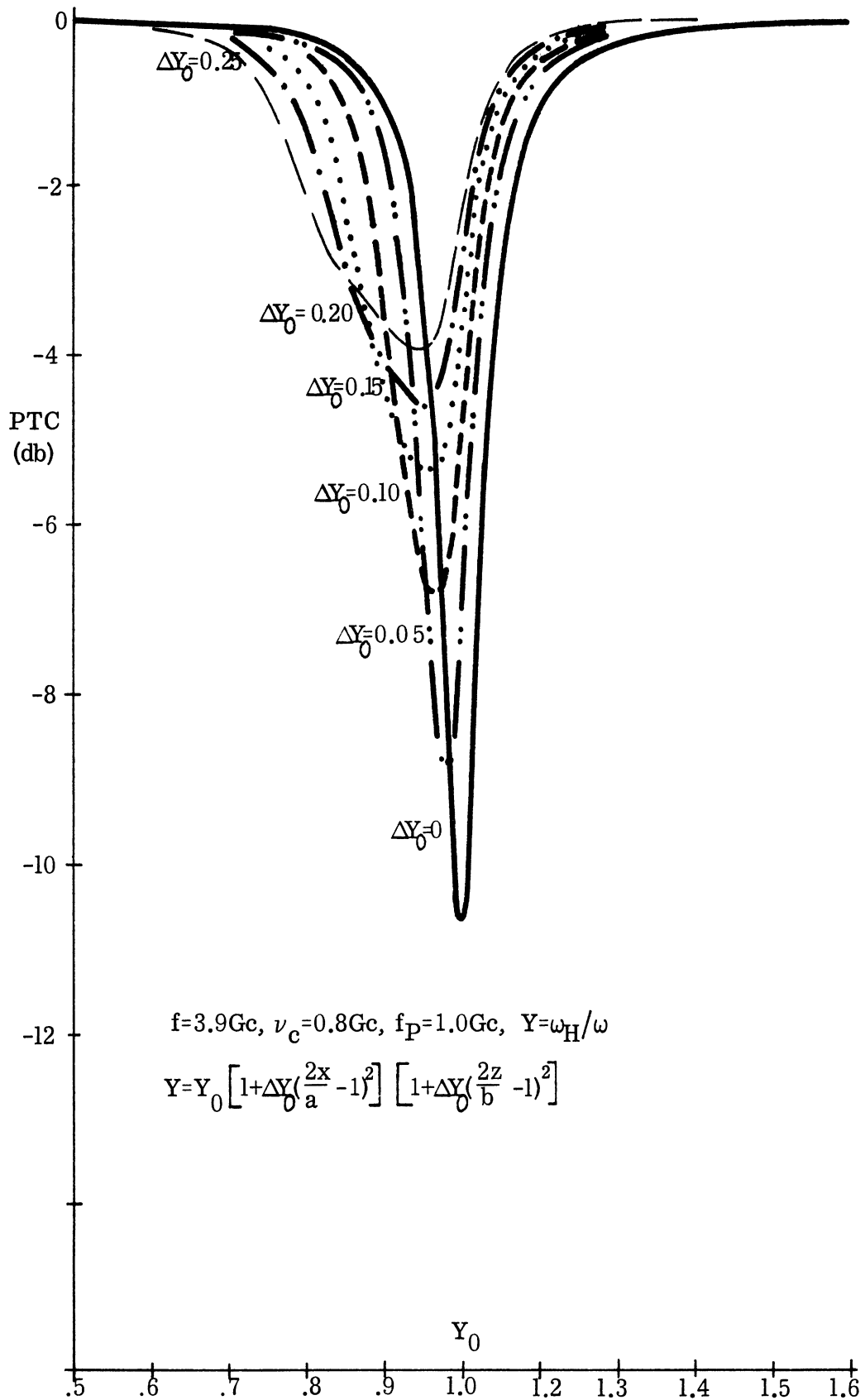


FIG. II-5: POWER TRANSMISSION COEFFICIENT AS FUNCTION OF Y_0 CALCULATED FROM EXTRAORDINARY WAVE APPROXIMATION WITH ELLIPTIC POLARIZATION ACCOUNTED FOR AND PARABOLIC MAGNETIC FIELD VARIATION

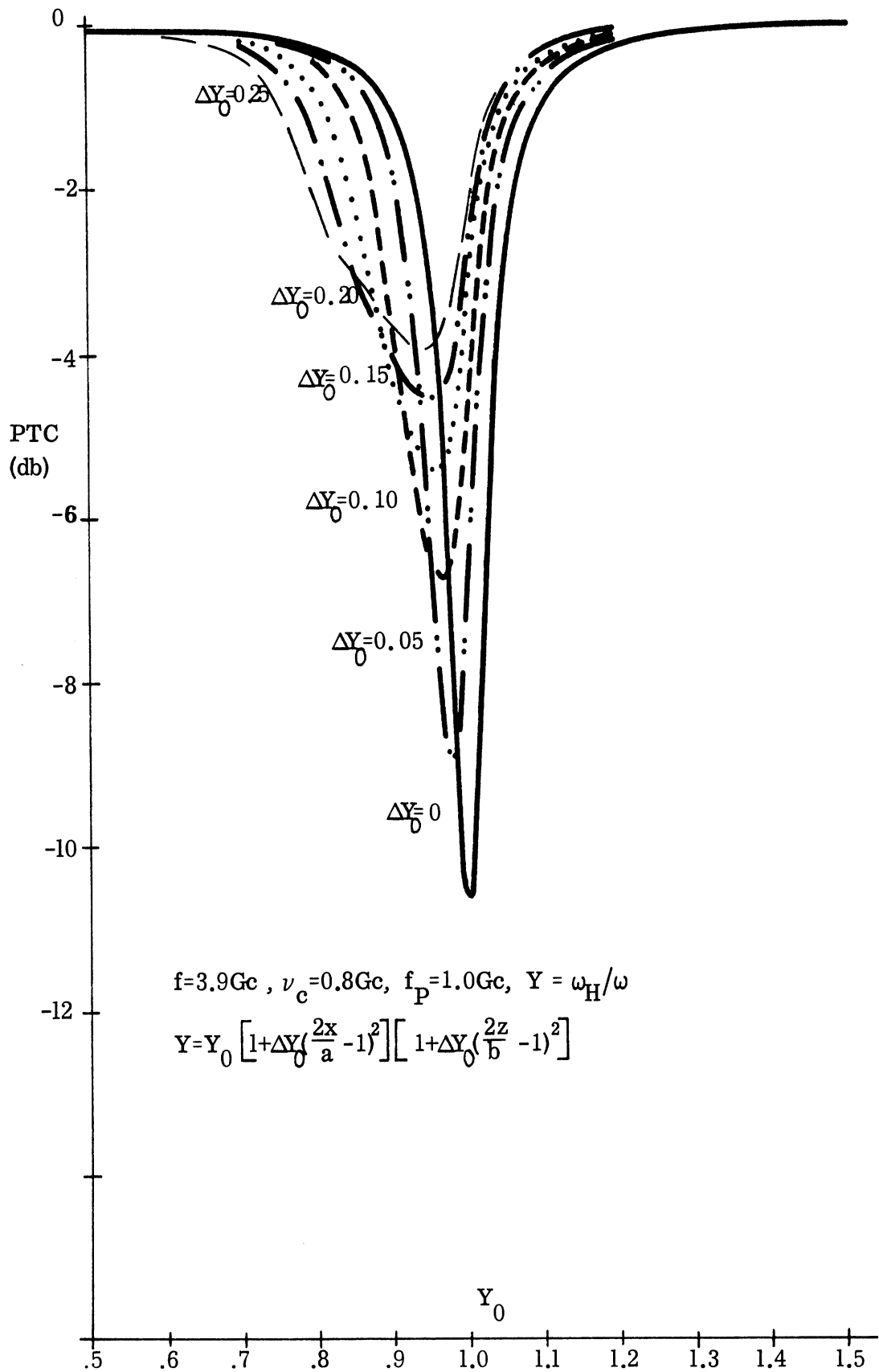


FIG II-6: POWER TRANSMISSION COEFFICIENT AS FUNCTION OF Y_0 CALCULATED FOR TENSOR PERMITTIVITY AND PARABOLIC MAGNETIC FIELD VARIATION

It is evident from these graphs that the tensor permittivity model and equivalent scalar permittivity model produce practically identical results for the ΔY_0 values used and the range of variables presented. One may see that in both representations P^2 appears as a factor, and therefore their equivalence holds for any P . For reasonably thin plasma slab and V^2 small compared to one both models are equivalent when Y is in the range $|Y - 1| < 0.5$ and being varied by the magnetostatic field changes. When Y is varied by the microwave frequency changes, then our calculations verify the agreement for $|Y - 1| < 0.2$.

Figure II-7 presents the relative decrease in the minimum power transmission coefficient as the non-uniformity of the static magnetic field is increased, i. e. ΔY_0 is increased. This calculation was carried out both for the tensor and the equivalent scalar model, and as expected from the previous discussion, both produced the same curve.

Comparison with Experimental Measurements

Some experimental measurements on an electron cyclotron resonance isolator were presented in a previous report (Olte, Miller, 1963). In particular, PTC data was presented for a variable microwave frequency at a fixed magnetic field strength, and for a variable magnetic field with a fixed microwave frequency. Some of this data is presented in Figs. II-8 to II-11 along with the corresponding theoretical results. The experimental curves represent the change in transmitted power due to addition of the plasma in the waveguide. The experimental curves are shown as continuous lines since they were obtained from sweep measurements.

The no-plasma insertion loss as a function of frequency is shown in Fig. II-8. The incipient absorption peaks are associated with mode conversion in the square waveguide section. As the two following graphs will show these resonances are strongly enhanced by the turning on of the magneto-plasma.

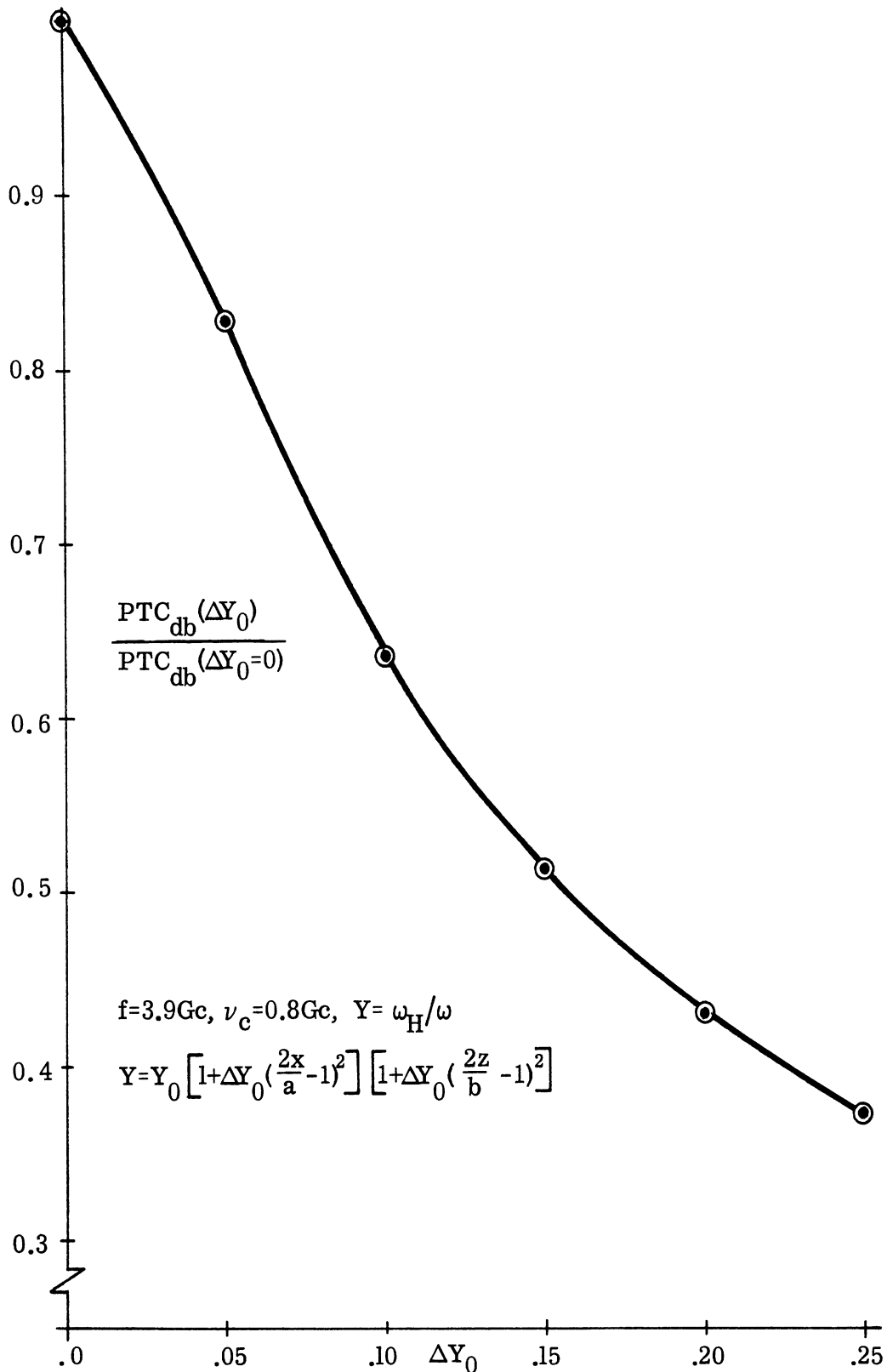


FIG II-7: RELATIVE DECREASE IN MINIMUM POWER TRANSMISSION COEFFICIENT AS FUNCTION OF MAGNETIC FIELD VARIATION OVER PLASMA VOLUME FOR BOTH EQUIVALENT SCALAR PERMITTIVITY AND TENSOR PERMITTIVITY

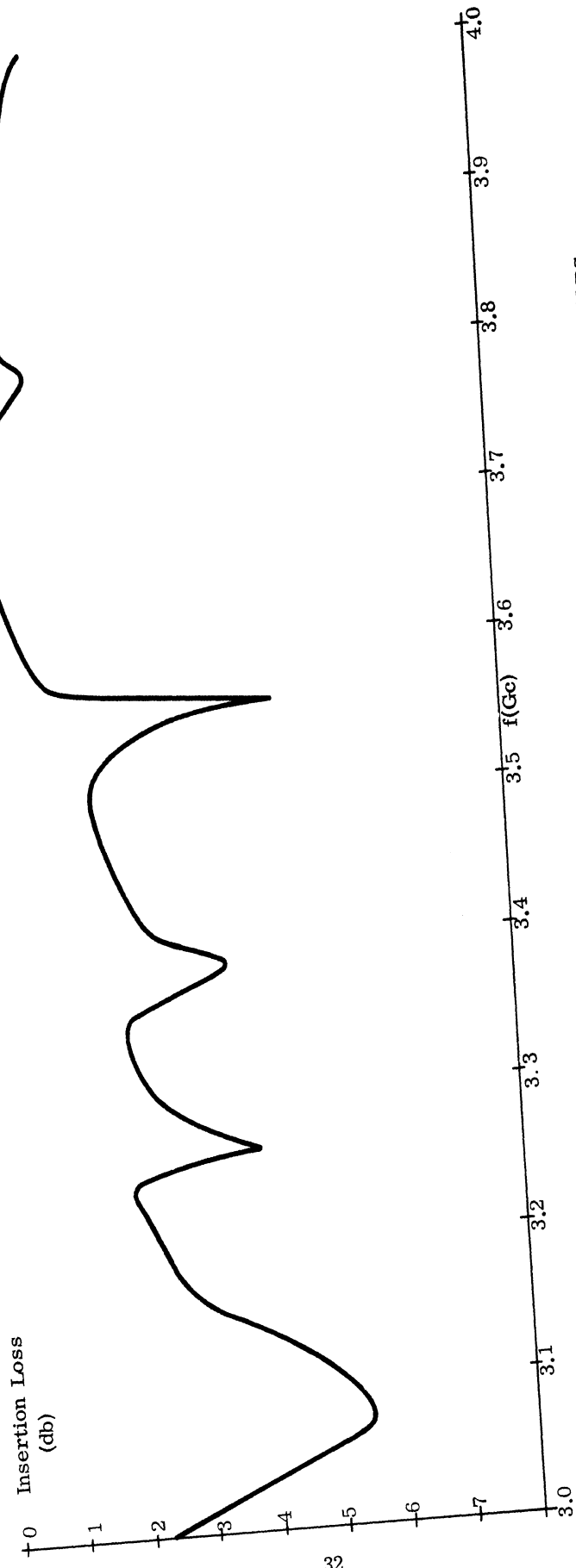


FIG. II-8: NO PLASMA ISOLATOR INSERTION LOSS WITHOUT MODE SUPPRESSORS

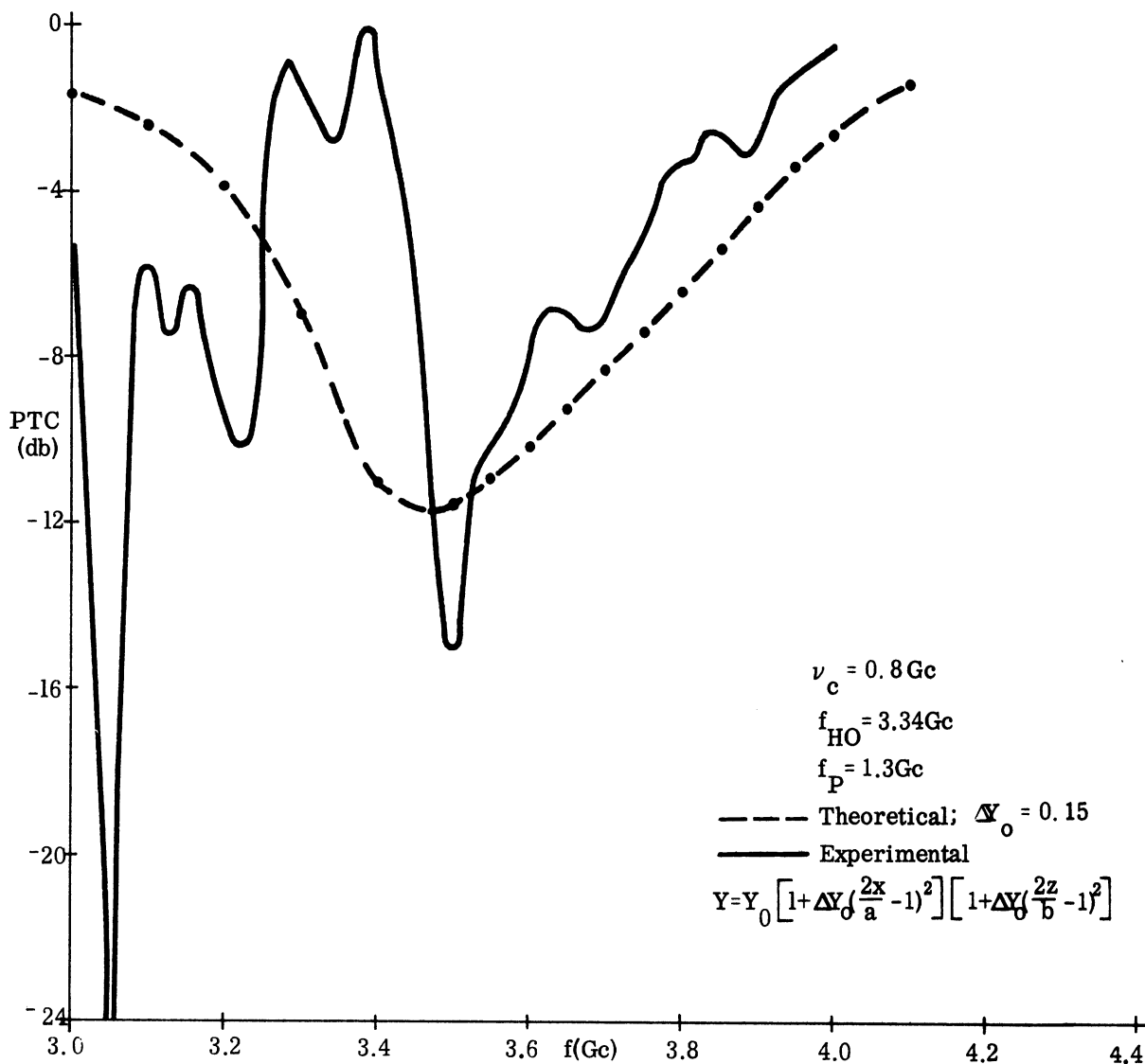


FIG. II-9: EXPERIMENTAL AND THEORETICAL POWER TRANSMISSION AS FUNCTION OF FREQUENCY. CALCULATED FROM TENSOR PERMITTIVITY AND PARABOLIC MAGNETIC FIELD VARIATION

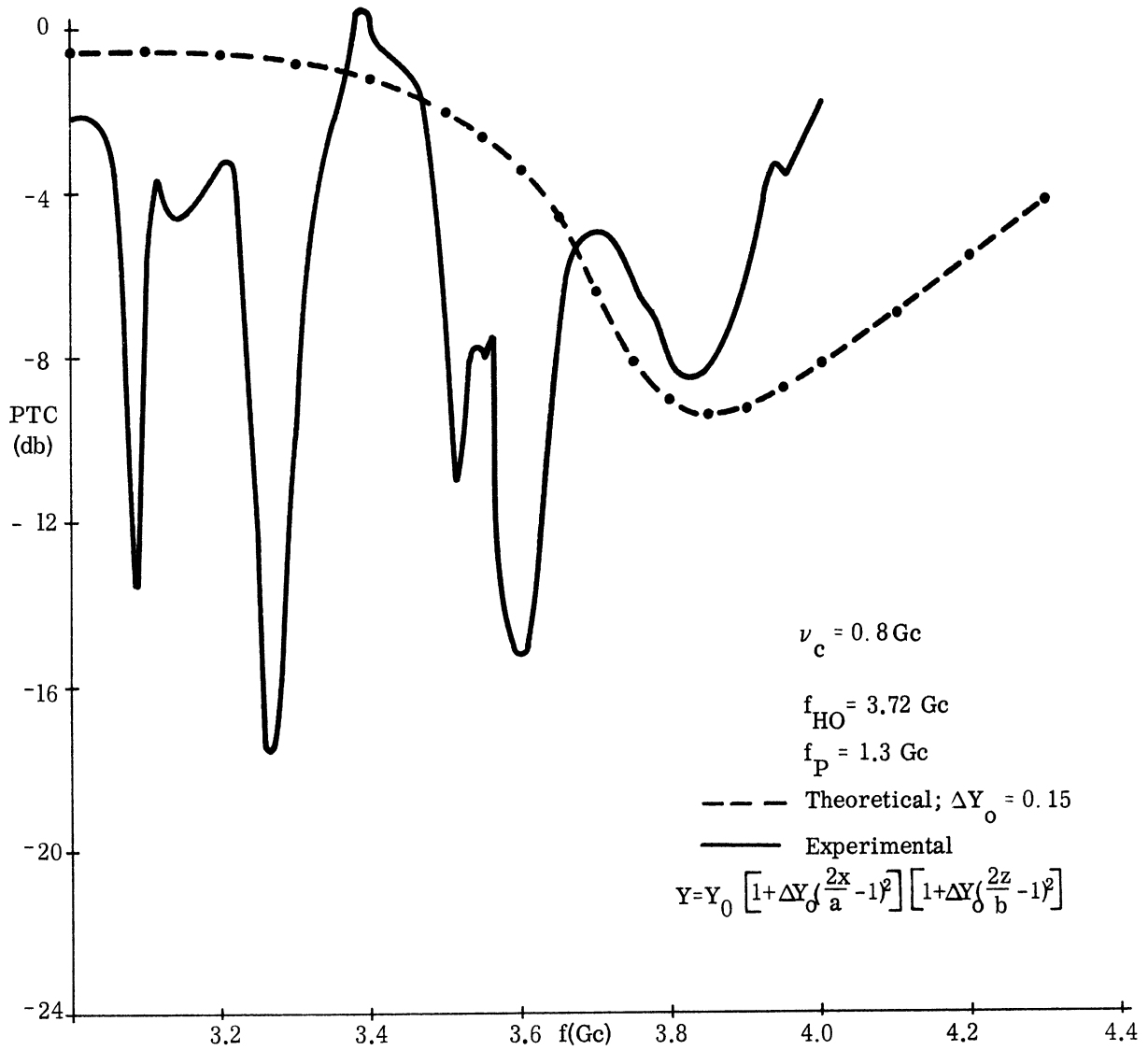


FIG. II-10: EXPERIMENTAL AND THEORETICAL POWER TRANSMISSION AS FUNCTION OF FREQUENCY. CALCULATED FROM TENSOR PERMITTIVITY AND PARABOLIC MAGNETIC FIELD VARIATION

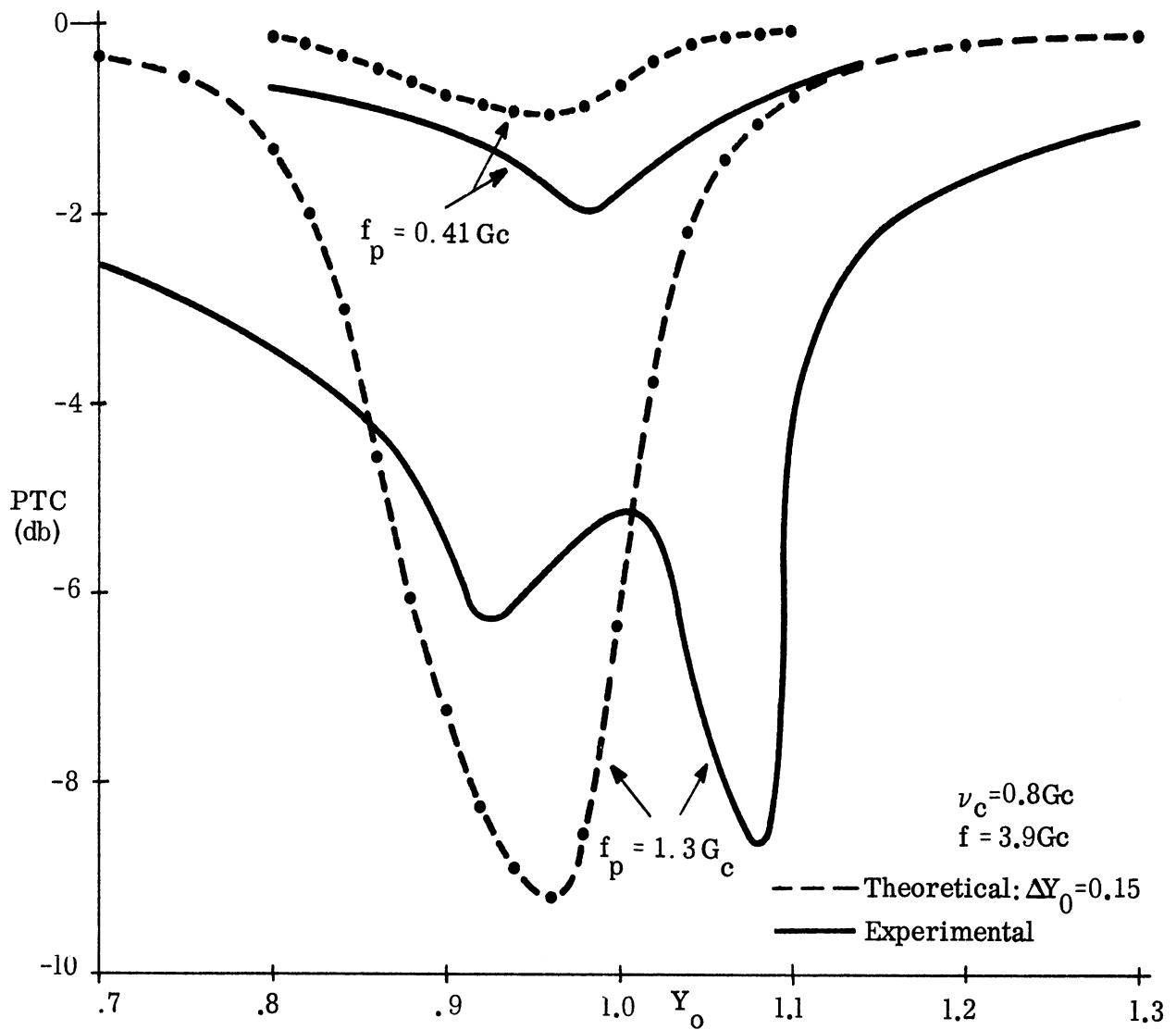


FIG. II-11: EXPERIMENTAL AND THEORETICAL POWER TRANSMISSION COEFFICIENT AS FUNCTION OF Y_0 . CALCULATED FROM TENSOR PERMITTIVITY AND PARABOLIC MAGNETIC FIELD VARIATION.

In Figs. II-9 and II-10 PTC curves are presented for $f_{\text{HO}} = 3.34$ Gc and 3.72 Gc respectively. The theoretical curves are for $\Delta Y_0 = 0.15$. The theoretical curves match only roughly some of the gross features of the experimental curves. All of the sharp absorption resonances come from the mode conversion and our theory does not take them into account.

Figure II-11 shows the plasma insertion loss when the magnetic field is the variable. The two sets of curves are for plasma frequency of 0.41 and 1.3 Gc. The theoretical curves are computed for magneto-static field inhomogeneities corresponding to $\Delta Y_0 = 0.15$. The microwave frequency is kept constant at 3.90 Gc which is in the middle of a frequency range free of mode conversion resonances.

The agreement between the theoretical and experimental data is much better than in the microwave frequency swept case. The amplitudes of the theoretical absorption peaks are in a reasonable agreement with the experimental peaks. However, they are displaced by $0.1 Y_0$. In the report by Olte and Miller (1963), the static magnetic field calibration using a Hall-effect Gauss-meter was 10 per cent too low and hence the apparent shift in the resonance peaks was $0.2 Y_0$. This large difference was suspected, and a recalibration of the magnet using a Gauss-Meter constructed on the nuclear magnetic resonance effect and having a 3 per cent accuracy, gave the present curves.

The magneto-static field calibration is good to within $\pm 0.05 Y_0$. In addition some displacement may be due to the type of static magnetic field inhomogeneities present. Thus the displacement is somewhat larger than can be accounted for by the measurement inaccuracies. Also the experimental absorption curve for the higher plasma frequency exhibits a double peak whereas the theory predicts only one.

In addition to the assumptions which were made in developing the theoretical analysis, there are some limitations on the parameters used in the theoretical

calculations. They are the static magnetic field strength, the electron plasma frequency, and the electron collision frequency. The characteristics of the first parameters encountered have been adequately discussed. We should make some comments on the last two parameters. These were measured independently by a microwave cavity resonance method. The shift in the resonance peak gave the plasma frequency, and the broadening of the resonance curve gave the electron collision frequency. The plasma frequency measurements were consistently within 10 per cent on various runs, while the collision frequency results varied by as much as a factor of two. These measurements gave us an effective average plasma frequency and an effective average electron collision frequency. This is an approximation in fact, because the plasma is inhomogeneous which must lead to a plasma frequency and electron collision frequency that depend on the space coordinates.

We have taken a model that is often used to explain qualitatively the electromagnetic wave absorption by the gyro-magnetic resonance in a plasma and put it in a mathematical form. Under some conditions, as we have seen, the model predicts the gross features of the microwave absorption reasonably well. Of course, when significant effects appear that are not included in the model, such as the mode conversion resonances, then the experimental results and the theoretical results diverge in some significant respects. The elementary model used suffers from many over-simplifications, and yet the other alternative - the full boundary value problem in this type of structure - is analytically so complex that one runs a strong chance of getting lost in numerical work without gaining any physical results.

Equivalent Circuit of the Cyclotron Resonance Isolator

We have developed a first order theory for the non-reciprocal absorption of the TM_{11} mode in a square waveguide that has a relatively thin transverse plasma slab parallel to the waveguide wall and spaced about one-quarter distance of the guide-width from it. The primary approximation in the theory is the neglect of the

electrical effect of the glass container of the plasma on the wave propagation, and the further assumption that the fields in the plasma have the same transverse variation as the TM_{11} mode fields in the empty guide. These approximations are not severe because the absorption is expected to exhibit a stationary character with respect to a variation in the fields. The non-reciprocal behavior of the device results from two facts:

- (1) $\epsilon_{ik}(\bar{H}_0) = \epsilon_{ki}(-\bar{H}_0)$, where \bar{H}_0 is the magnetostatic field, and
- (2) the magneto-ionic plasma slab is placed in an asymmetric position with respect to the magnetic fields of the TM_{11} mode.

An implicit assumption in the theory is that only the TM_{11} mode may propagate. But, in our case we have a multimode waveguide; the lower order modes TE_{10} and TE_{01} may propagate as well. However, in the circuit for which we are using the solution we have only a section of the square waveguide which contains the magneto-ionic package. On both ends of this section are the TEM- TM_{11} mode transducers, as shown in Fig. II-12. In the same figure we have also presented an equivalent microwave circuit which represents the main features of interaction of the waves with this structure. Starting from the left hand side of the circuit we have elements as discussed below. The TEM mode of the coaxial line is represented by an ideal transmission line of characteristic impedance, Z_0 and the propagation constant $j\beta_0$. Both constants are real. If the reference planes are selected properly any loss-free two-port network may be replaced by an ideal transformer. We have chosen to so present the TEM to TM_{11} mode transducer. The section of the square waveguide between the mode transducer and the magneto-ionic package is represented by ideal transmission line of characteristic impedance Z_1 , and phase constant $j\beta_1$, both again real. This representation is with respect to the TM_{11} mode. The section of the square guide containing the magneto-ionic package

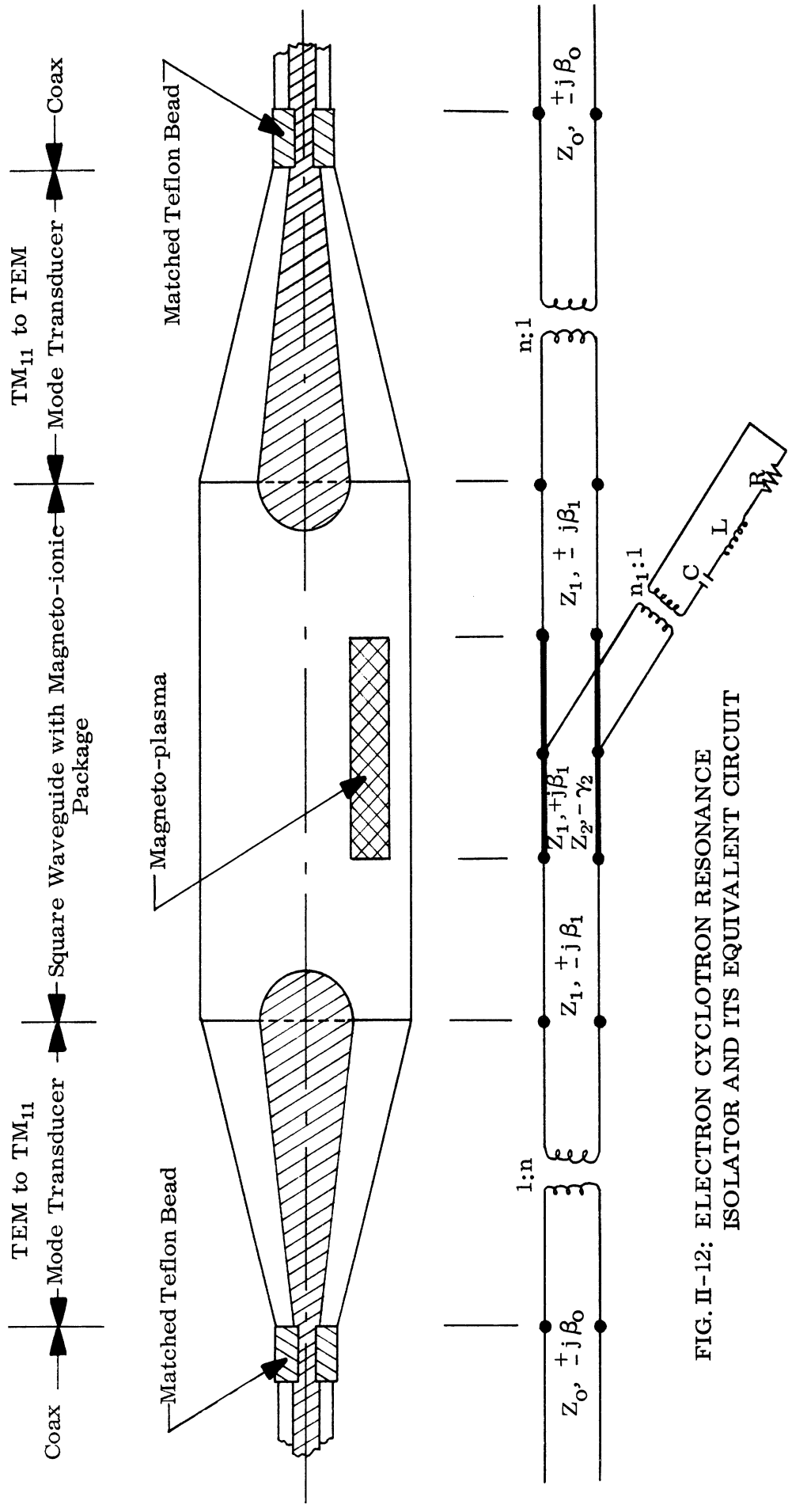


FIG. II-12: ELECTRON CYCLOTRON RESONANCE ISOLATOR AND ITS EQUIVALENT CIRCUIT

is represented again with respect to the TM_{11} mode by a non-reciprocal transmission line. When the propagation is from left to right, both the characteristic impedance, Z_2 , and propagation constant γ_2 , are complex and the wave suffers attenuation. For propagation from right to left however, the magneto-ionic package is practically invisible to the wave, and hence the transmission line parameters are the same as for the empty square guide. If the magnetostatic field was reversed, then the non-reciprocal transmission line would also reverse. Since the structure is symmetric with respect to a transverse plane passing through the center of the plasma package, the equivalent microwave circuit to the right of the plasma package consists of an ideal transformer connecting two loss-free transmission lines. This is the same type of circuit as to the left of the magneto-ionic package which already has been discussed. One really should include a coupling network on the ends of the non-reciprocal transmission line. In a general case the network should be a 'T' network. However, in some more elementary, but similar situations where the problem has been worked out (Collins, 1960), the effect of this network on the wave propagation is of practically insignificant importance. Therefore, in our case it is reasonable to neglect it as well.

This would be the end of the story of the equivalent microwave circuit of the device if the square waveguide were a single mode guide. On the contrary, it may also propagate the TE_{10} and TE_{01} modes in addition to the TM_{11} mode. However, these modes are axially asymmetric and therefore the TM_{11} to TEM mode transducer will not convert them into a TEM mode. But this is the only mode which is allowed to propagate on the co-axial line. Thus we have a situation in which the mode transducers form shorts on both ends of the square waveguide section as far as the TE_{01} and TE_{10} modes are concerned. In effect, we have a cavity in which may exist TE_{01n} and TE_{10n} resonant modes; n in our case being an appropriate integer. These modes may exist only for certain microwave frequencies. At these

resonant frequencies the resonant modes will be coupled by the plasma package to the TM_{11} mode. That means that energy will be taken from the travelling mode and dissipated primarily in the wall losses of the resonant mode fields. The coupling will occur only for the direction of travel in which the plasma section of the guide appears lossy to the TM_{11} mode.

To take into account the power loss out of the TM_{11} mode due to these coupled cavity resonances we have included a series resonant circuit which is coupled by an ideal transformer to the center of the lossy transmission line. It is doubtful that this part of the circuit may be justified rigorously, but the inclusion of the present model appears not only reasonable, but also necessary. Because the cavity walls and the plasma package itself dissipate energy out of the resonant cavity mode we have included a resistor in the series resonant circuit. The inductance, capacitance, and resistance is determined by the character of the resonant mode fields and the electrical energy dissipation in the cavity. The coupling transformer with turns ratio n_1 we have chosen to interpret in such a way as to introduce the nature of directivity in the resonant mode excitation. When the TM_{11} mode is travelling from left to right, then n_1 is of some appropriate finite value; for the opposite direction of TM_{11} mode travel we have no coupling and hence $n_1 = \infty$.

When the frequency of the TM_{11} mode is not within line width of any coupled cavity resonance, then the series resonant circuit presents a large impedance to the transmission line and hence its loading effect on the transmission line is negligible.

III

EXPERIMENTAL WORK ON PLASMA PACKAGE

Introduction

An experimental investigation into possible plasma applications in microwave circuits was recently carried out at this laboratory (Olte and Miller 1963). In that investigation one of the plasma configurations used consisted of a rectangular plasma slab placed across a square waveguide with its broad side parallel to one of the waveguide walls. The plasma was generated as a cold discharge using argon gas. A static magnetic field was applied parallel to the plasma slab, making the plasma an anisotropic medium, so that the waveguide section containing the plasma acted as an isolator of guided electromagnetic waves.

The present investigation was undertaken for the purpose of developing a stable and convenient plasma package suitable for use in such plasma-microwave circuits. Due to the limitations on current density (and thus electron plasma frequency) and the well-known but little-understood oscillations and instabilities of the cold cathode discharge, it was decided that a hot cathode discharge be used for this purpose. The disadvantages of the hot discharge compared with the cold discharge are the requirement of an additional power supply for heating the cathode, evaporation of cathode material onto the walls of the tube, and the requirement of a very high gas purity to avoid cathode poisoning. Its advantages over the cold discharge are higher discharge current, lower anode voltage, and no significant sputtering problem. In addition, it was felt that due to the lower operating voltages, the hot discharge would exhibit greater stability than the cold discharge.

We decided that the most useful plasma geometry would be in the form of a slab. This seems to be the most suitable package shape for waveguide applications. It was anticipated that the isolator mentioned above would be the first device to utilize the hot discharge plasma, so the dimensions of the glass envelope were chosen accordingly.

After considerable experimentation in the fabrication of a rectangular glass envelope, the glass blower was successful in developing a method for making envelopes of a uniform size. The main body of the envelope was made by cutting a section of wall from a large pyrex beaker and folding this over on itself so that a cylinder of almost rectangular cross section, rounded at the edges, was formed. A $1\frac{3}{8}$ in. diameter cylinder of glass, closed at one end and having a slot cut into its side as wide as the rectangular section was thick, was attached to one end of the rectangular section. A similar cylinder of glass 1 in. in diameter was attached to the other end. A standard 8-pin tube base with feed through pins 0.050 in. in diameter and with the cathode assembly mounted on it was fitted to the open end of the larger cylinder, and the anode mounting similarly connected to the smaller cylinder. The cathode and anode assemblies could thus be removed, and the envelope cleaned and re-annealed for further use.

As a result of previous experience with oxide coated cathodes and some work with thoriated tungsten cathodes in the initial phase of the present investigation, a barium-nickelate cathode was chosen for use in the first experimental plasma tubes. This cathode has an operating temperature of 850 to 950^o C, an emission of 2 to 3 amperes per square centimeter, and is more impervious to ion bombardment than either the oxide or thoriated tungsten cathodes. The cathodes which we used were supplied to us as engineering samples by the General Electric Company and were modified by us for our application.

Material chosen for the anode, heat shield and auxiliary components in the tube was either a special high purity nickel, for parts of the tube which would operate above the Curie temperature of nickel (the tube would be placed in a strong magnetic field when used in the isolator), platinum or tungsten. Platinum was also used for making some of the welds. Some ceramic bead insulators were used in the earlier designs.

Great care must be taken that the components being used in a hot cathode tube are cleaned by the proper degreasing and firing procedures to avoid cathode poisoning once the tube is assembled. Materials that had been prepared for use in a tube were stored in a desiccator containing a drying agent until they were needed. In addition, the evacuation of the tube must be accomplished without harmful contamination from the pumping station.

A glass manifold was built for tube evacuation and was used with an ion-pump which was available in our laboratory. However, the ion-pump failed shortly thereafter, so a new station was built using a 2 in. diffusion pump with a mechanical fore-pump. A glass and metal manifold was designed for use with the new vacuum station. When a simple diode containing a thoriated tungsten cathode was evacuated on this system, the cathode was quickly poisoned. The poisoning was determined to be due to the stop-cock grease used in the glass parts of the system, and possible leaking of the stopcocks. The stop-cock grease has a vapor pressure less than 10^{-6} Torr at room temperature, so this indicates how susceptible cathodes are to poisoning by petroleum derivatives. Thus an all metal, stainless steel manifold was assembled and found to give satisfactory service in subsequent operation.

Inquiries were made at the various suppliers of research grade gases for gases of maximum purity. The most damaging contaminates from the viewpoint of cathode poisoning would be oxygen and compounds of oxygen. No information could be obtained on the maximum allowable oxygen content in which a hot cathode could be operated before poisoning would become a problem. The purest gases available contained on the order of 5 parts per million oxygen and 10 parts per million of oxygen compounds. We ultimately used Matheson research grade gases, supplied in 1 liter glass bottles at 1 atmosphere pressure.

Experimental Results

Vacuum System

A diagram of the all-metal vacuum system which was in use during the development of the discharge tubes described below is shown in III-1. The only portions of the manifold which are not bakeable at temperatures greater than 100°C are the two one-inch Varian valves. These valves contain Viton O-ring seals.

Flexible heating tapes were wrapped around the rest of the manifold and fittings, so that bake-out temperatures of 200°C could be achieved. The demountable parts of the system are connected with Varian flanges and copper gaskets while the permanent connections are made with soft silver solder joints. The gas bottle is connected by means of a copper tubulation compression fitting. A 1 in. diameter Kovar-glass adaptor is employed for connecting the plasma envelope to the system.

Small silver-soldered diaphragm needle valves are used for the gas inlet, a line to pump around the diffusion pump, and the air inlet. Two valves are used in series for the air inlet, and the line between them kept evacuated to minimize leakage.

A magnevac sensing gauge is used for vacuum measurements from atmospheric pressure to 10^{-3} Torr and an ion gauge for the range 10^{-3} to 10^{-8} Torr. Safety circuits are included that shut off the diffusion pump if the pressure exceeds approximately 10^{-2} Torr. The mechanical pump then turns off three minutes later if the pressure has not decreased to less than 10^{-2} Torr. These precautions are taken to avoid damaging the diffusion pump oil and the mechanical fore pump.

A water cooled baffle is located between the diffusion pump and manifold, to minimize back streaming of the diffusion pump oil. When, after three months' operation, the manifold was taken apart for cleaning, there was no evidence of oil deposition upstream from the diffusion pump. Pressures as low as 5×10^{-7} Torr have been obtained with this system, after bakeout at temperatures of 150° to 200°C.

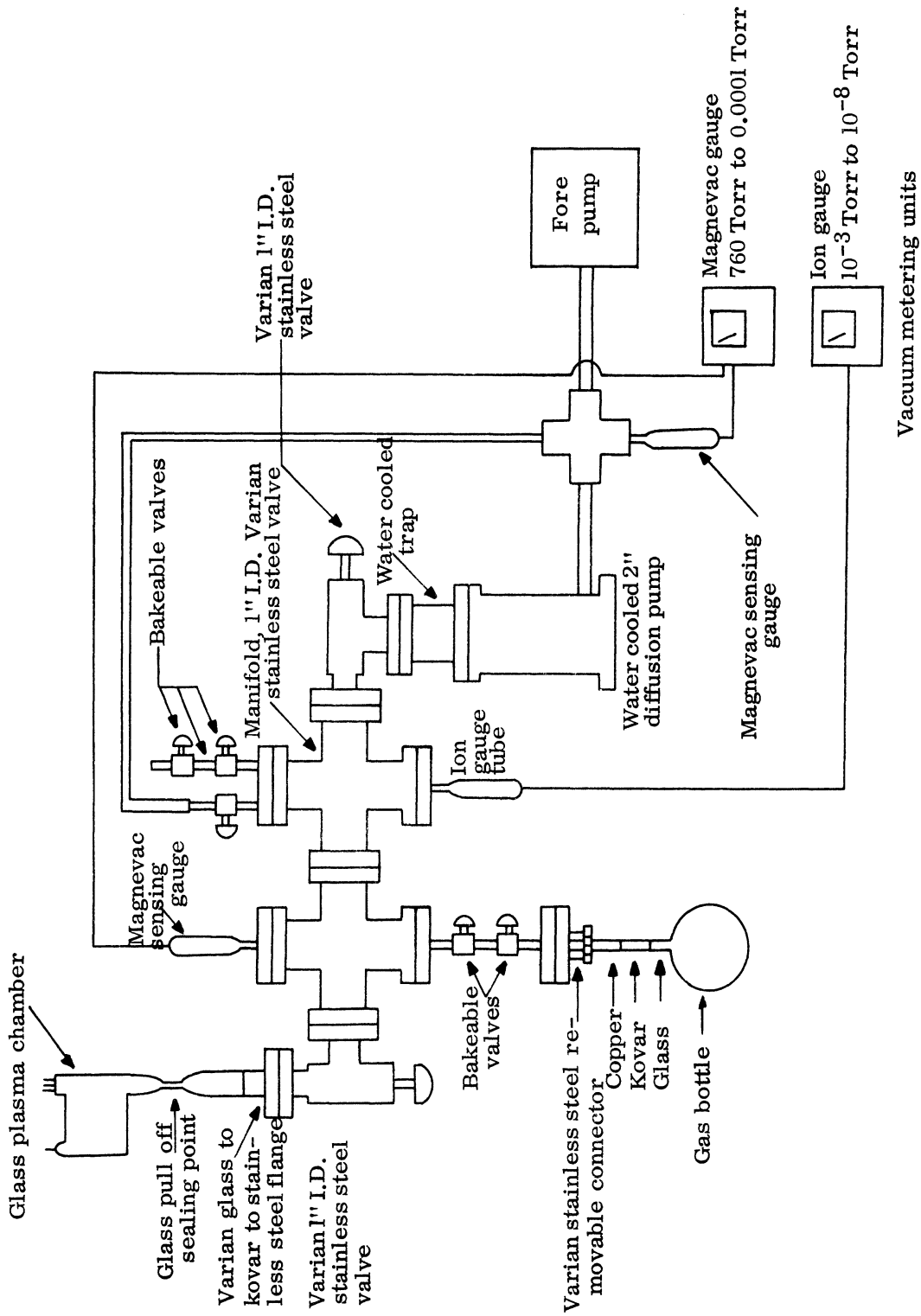


FIG. III-1: SCHEMATIC OF ALL METAL VACUUM SYSTEM
 (All Above Varian Flanges use Copper Sealing Gaskets)

Discharge Tube

A picture of the first discharge tube is shown in III-2. The tube envelope is 5 inches long overall by $2 \frac{7}{8}$ inches wide, has a center thickness of $1 \frac{3}{8}$ inches, and thickness at the edges of about $\frac{3}{4}$ inch. The side walls of the tube are convex outward for strength so that seen from the end, the tube looks like a truncated ellipse, of high eccentricity. The glass walls are about 0.1 inch thick. Four other tubes were subsequently built and for purposes of convenience the tubes will be numbered 1 to 5. While the envelopes remained unchanged, there were some differences in the arrangement of the elements within the individual tubes.

In all the tubes, the cathode and anode are placed parallel to the narrow ends of the tube and separated by a distance of about $3 \frac{3}{4}$ in. The anode consists of a piece of tungsten or platinum about $2 \frac{1}{4}$ in. long by $\frac{1}{2}$ in. wide. The differentiating features of the various tubes are discussed below.

Tubes 1 and 2 were identical. Each had a box-like heat shield of nickel sheet 0.005 in. thick at the cathode end of the tube placed so that the open side faced the anode. It was supported by nickel wires welded to feed through pins. The cathode itself was recessed within the heat shield and supported at its ends and center. The lower end of the cathode was welded to a nickel lead wire connecting to a feed through pin, while the other end was welded to the heat shield which served as a second lead. Ceramic bead insulators were used to stand off the cathode from the heat shield at the center support. The cathode as seen along the axis has the shape of a semi-circle closed along the diameter with the flat part facing the heat shield. The front and back surfaces are cut by slots which are aligned with each other. Platinum foil, 0.002 in. thick and welded to a tungsten feed-through rod 0.035 in. in diameter served as the anode. A getter was mounted back of the heat shield. The cathode area was 3 in.^2 and at operating temperature the heater power was 90 watts.

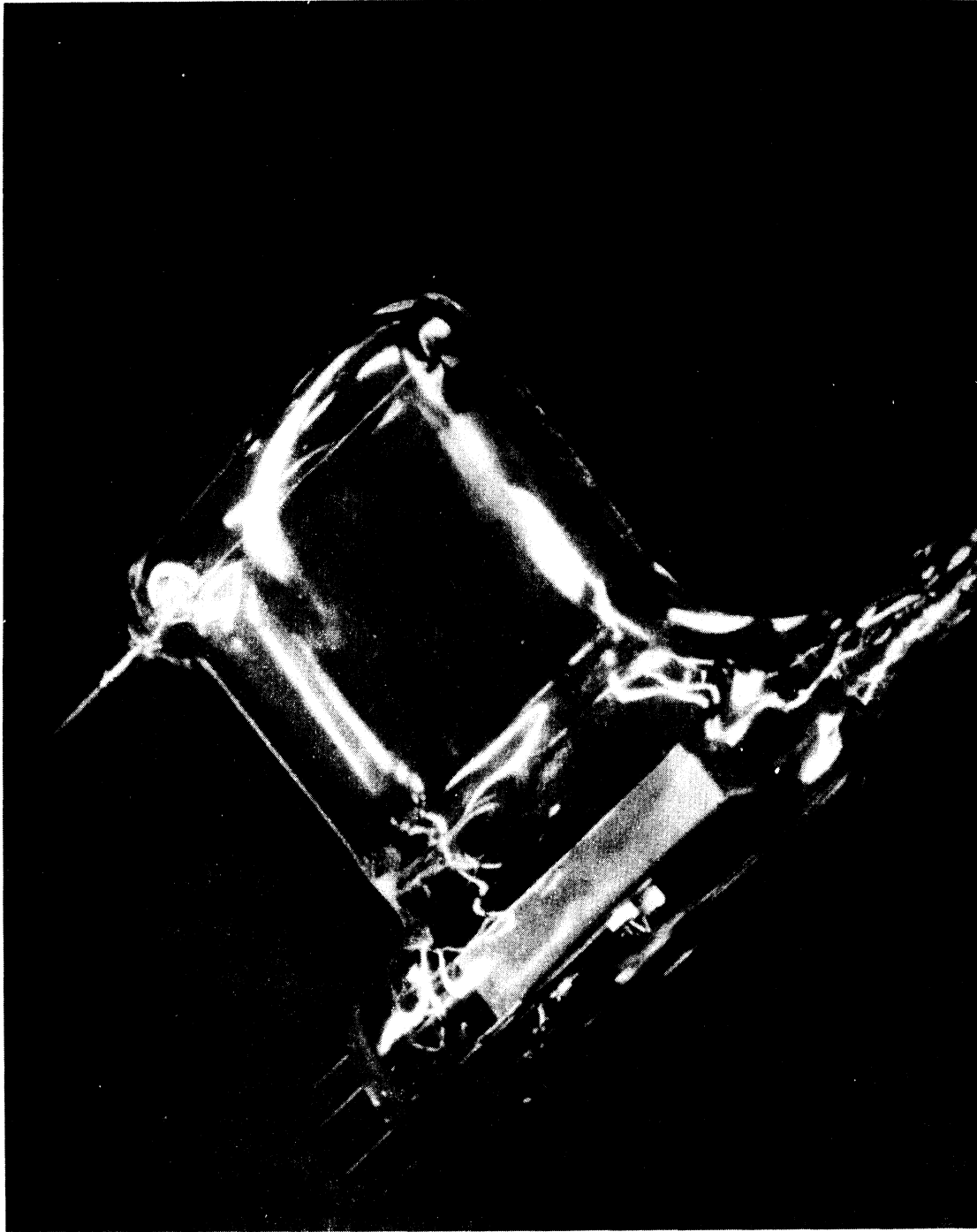


FIG. III-2: THE PLASMA PACKAGE

Tube 3 incorporated a tungsten anode 0.005 in. thick. A heat shield consisting of a flat piece of nickel sheet 2 1/2 in. long by 3/4 in. wide and 0.005 in. thick slightly beveled along the longer edges was used. The cathode was constructed of two parallel strips of barium-nickelate coated nickel 1/8 in. in width and 2 1/2 in. in length. It was supported at one end by nickel lead wires connected to feed-through pins in the tube base, and at the other end by the heat shield. The cathode area was 1 1/4 in.² and the heater power was 75 watts.

Tubes 4 and 5 were also identical and a tungsten anode was again used. The anode was spaced 3/16 in. from the feed-through rod by four nickel wires 0.020 in. in diameter. This arrangement was used because experience with the preceding tubes had shown that the anode became red hot at the higher discharge currents. So long as the anode was in full contact with the feed-through rod, there was the danger that the glass around the feed-through would crack or melt at high anode temperatures. In this way, however, the anode was thermally insulated from the feed-through. The cathode in these tubes consisted of a single strip of 1/8 in. wide cathode material 2 1/2 in. in length. No heat shield was used, but a nickel wire was inserted about 1/8 in. in front of the cathode for use as an auxiliary anode to aid in activation. The cathode area was 5/8 in.² and the heater power about 48 watts.

The development procedure which was followed was basically the same for all tubes. After the cathode and anode assemblies were built, they were stored in a dessicator until a tube was needed. As soon as they were mounted in an envelope (except in the case of Tube 1) the completed tube was put on the manifold and pumped down. A bake-out period of 72 hours or longer followed at temperatures up to 350° C. Manifold pressure during bake-out was generally below 10^{-4} Torr.

Cathode activation was then begun. The cathode current was gradually increased in such a way as to keep the manifold pressure below 5×10^{-4} Torr. After the cathode temperature had been raised to about 900° C as measured by an optical

pyrometer, and the pressure had decreased to less than 5×10^{-6} Torr, the cathode current was increased by 50 per cent for a period of 10 minutes. Hydrogen gas at a pressure of approximately 0.5 atmospheres was let into the envelope then, and the cathode maintained at a temperature of about 850°C , for a period of 15 to 20 minutes. This last step should have completed the cathode activation, but we found that further flashing as well as operating the cathode in a hydrogen discharge resulted in increased emission. After a few hours operation in the hydrogen discharge the cathode had become hardened to the point where increasing the cathode temperature from ambient to operating value produced no increase in manifold pressure. The manifold pressure, after cathode activation and with the tube on the system, was generally 10^{-6} Torr or less.

Before the overall experimental data are presented, the results obtained with each tube are briefly summarized here.

Tube 1

This tube was not successfully activated since it had been evacuated on the glass and metal manifold and the stop-cock grease evidently contaminated the cathode. It did serve however, to test the general design and showed that the cathode heater current was higher than expected. This led us to provide additional feed-throughs for the cathode circuit to accommodate the higher currents in the second tube.

Tube 2

The cathode was activated although with some difficulty and a series of phase shift measurements at S-band were carried out using hydrogen gas for the discharge. Some problems in the discharge characteristics were encountered which were thought to be due to the cathode geometry. This led to a redesign of the cathode arrangement for the third tube.

Tube 3

This cathode was easily activated. Some phase shift data was obtained using a hydrogen gas discharge, but the cathode life proved to be quite short as one small section got considerably hotter than the remainder of the cathode. It eventually melted away, opening the cathode circuit.

Tube 4

Activation of the cathode was accomplished and an extensive series of phase shift measurements was taken at X-band using a hydrogen discharge. Measurements were also obtained using Xenon gas. The cathode developed a hot spot similar to that of Tube 3 and evaporation of cathode material eventually caused this cathode to also melt open.

Tube 5

Activation of the cathode was routinely accomplished and additional data was obtained on the hydrogen discharge characteristics. The envelope cracked and was successfully repaired without apparent damage to the cathode. Just before the tube was to be removed from the manifold, the envelope again cracked and was damaged beyond repair.

All discharge data presented here was taken while the tubes were mounted on the manifold. It had been thought at first that the cathode would poison if this were attempted due to the accumulation within the manifold and tube of air leaking in while the pump was valved off. However, data runs of two and three hours duration were carried out with no noticeable cathode poisoning. When the manifold alone was valved off from the pump, the pressure rose from 2×10^{-6} Torr to 3×10^{-4} Torr in ten minutes and then remained between 3 and 4×10^{-4} Torr for the duration of the test (one hour and twenty minutes).

Tubes 2 and 4 were filled with hydrogen and xenon gas respectively and removed from the system. A getter was fired in Tube 2, following recommended

thyatron tube procedure, but no discharge could then be started. It was determined that the getter was much more efficient than was anticipated, and had pumped the tube down from about 1 Torr (the original fill pressure) to less than 10^{-2} Torr. Tube 4 was operated for eight and one-half hours after removal from the system, when its cathode burned open. During this time the operating voltage increased by a factor of more than 2, but whether this was due to cathode poisoning, or evaporation of the cathode is not known.

Diagnostic Technique

A considerable amount of effort was expended in devising a suitable diagnostic technique for investigating the discharge properties. While a resonant cavity technique had been successfully employed for finding the electron plasma frequency and collision frequency for the cold discharge used in the cyclotron resonance isolator mentioned previously (Olte, Miller, 1963), this technique could not be used in this situation due to the tube geometry.

The tube is large enough that the highest possible TE_{011} mode resonant frequency would be slightly above 2 Gc. Thus only plasma frequencies less than 2 Gc could be measured. It was anticipated that plasma frequencies considerably higher would be obtained in the hot cathode discharge.

Use of a Langmuir probe was ruled out because it would interfere in any later operation of the tube. Furthermore, it could not be used without disturbing the plasma.

An interferometer technique was decided upon. Some preliminary measurements were taken at 2.2 Gc using Tube 2 and a hydrogen discharge. The results obtained were inconclusive. Leakage of radiation around the tube decreased the sensitivity of the measurements and the tube geometry may have contributed to uncertainty in the data.

To avoid these problems an X-band interferometer operating at 10.6 Gc was set up. The transmitting horn with a $3 \frac{1}{2} \times 3$ in. aperture was placed $1 \frac{1}{4}$ in. from the glass wall. An open ended X-band waveguide on the opposite side and $\frac{1}{8}$ in. from the glass wall was used as a receiving horn. Both horns were aligned midway between the ends of the tube. To check out the interferometer geometry a spare tube envelope was filled first with benzene and then with salt, and the phase shift due to the introduction of these substances was measured. A theoretical phase shift was calculated using as a model a plane wave incident on three dielectric slabs infinite in extent in a direction normal to the direction of propagation, and having thicknesses of 0.1, 1.0 and 0.1 in., respectively. The 0.1 in. thick slabs represent the glass walls of the tube and the 1.0 in. thick section corresponds to the dielectric which fills the tube. When the appropriate dielectric constants for the glass, benzene and salt were used, the measured phase shift for the benzene fill was about 16 per cent greater and that for the salt about 14 per cent less than the theoretical values. Since the measured values lay on both sides of the theoretical results by about the same amount, the theoretical model was accepted as reasonable.

This same model was then used to calculate the phase shift when the center dielectric is a plasma. Bachynski, et al (1963) discussed this model and some of their results were used. Fig. III-3 shows the calculated phase and amplitude of the transmitted signal as a function of the normalized plasma frequency P . It was assumed that $\nu_c \ll \omega$. This should be a reasonable assumption based on the gas pressures used. A value of ν_c / ω as large as 0.1 would not greatly change the phase shift across the plasma.

Electron densities in the discharge were obtained from the curves of Fig. III-3 using the interferometer data. The phase shift data was used primarily for this purpose, but the attenuation results were used when the signal was attenuated by more than 5 db, or when P exceeded 0.9. The leakage radiation around the discharge tube was measured at 33 db below the radiation passing

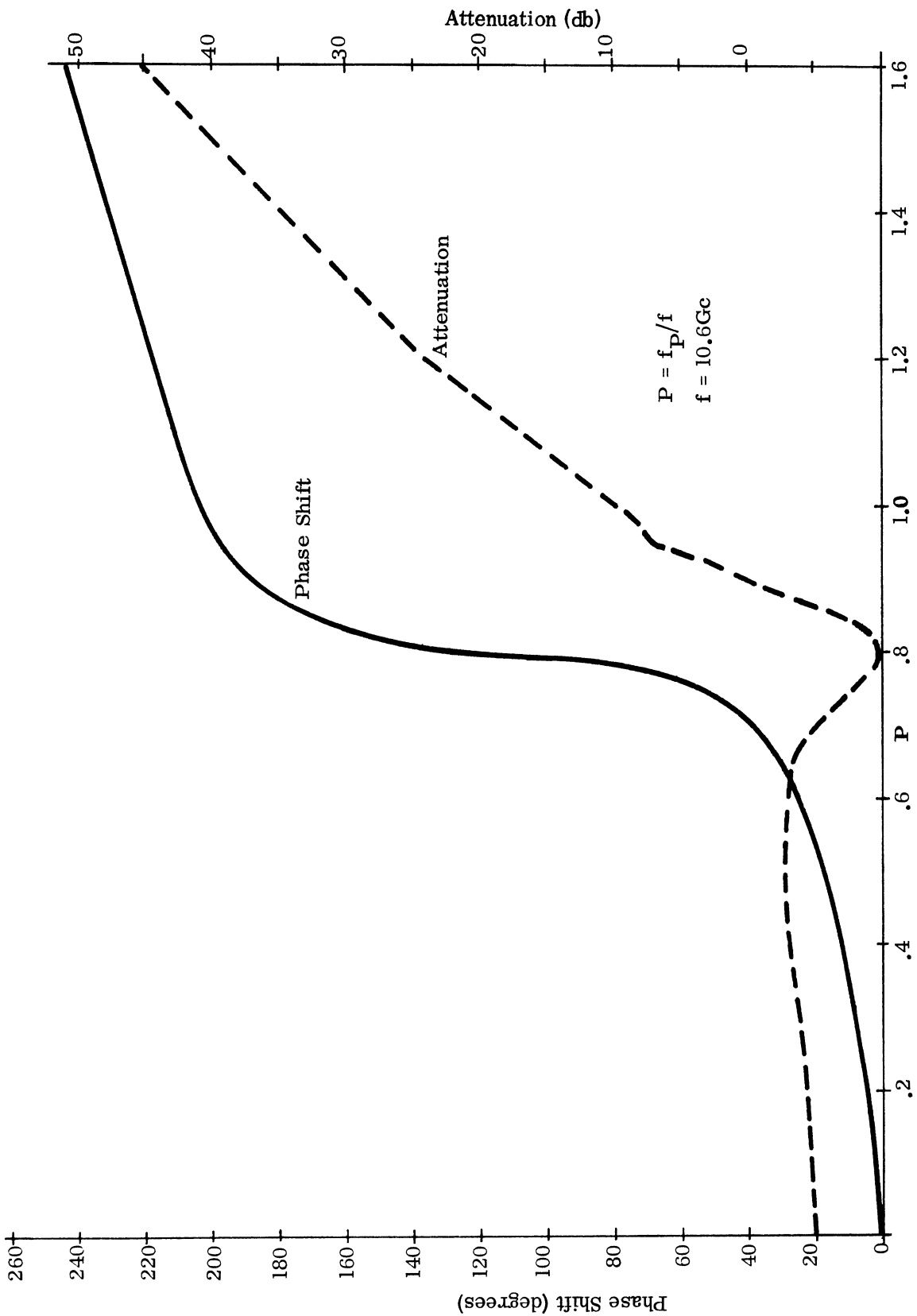


FIG. III-3: THEORETICAL PHASE SHIFT AND ATTENUATION ACROSS 1 INCH PLASMA SLAB CONTAINED WITHIN 0.1 INCH GLASS PLATES AS A FUNCTION OF P

through the tube. This means that meaningful interferometer results are probably limited to values of P of 1.2 or less.

Hydrogen Discharge

Fill pressures between 0.02 Torr and 1.0 Torr were used. Most of the data was taken at 0.40 Torr. At the lower fill pressures, the hydrogen discharge generally appeared as a fairly uniform, bluish glowing gas with a well defined boundary between the glow and a dark space midway between the cathode and anode.

The dark space gradually merged to a bright glow surrounding the cathode. Another less well-defined dark space was located near the anode. The glow appeared to fill the entire cross-section normal to the current flow. Increasing the current brightened the area surrounding the cathode and widened the center dark space. At current less than 20 ma, the glow was very tenuous but seemed to fill the envelope uniformly.

As the fill pressure was increased, well-defined striations formed. The glowing gas in the striations had a deep blue color in a thin layer on the side nearest the cathode, sharply differentiated from the remainder which was a reddish blue color. The striations changed in thickness and location with the discharge current.

Abrupt changes were sometimes observed in the discharge appearance. The discharge seemed to change modes as the current was increased, having a quite uniform appearance for currents less than 20 ma and a banded structure for larger currents. Oscillations were frequently observed in the glow pattern. These were sometimes attributed to more actively emitting spots on the cathode, as the glow flickered about, originating from various localized cathode areas. Frequently, the discharge of Tubes 3 and 4 formed a beam spreading out from a particular location on the cathode which was noticeably brighter than the surrounding area. The discharge mode could be changed only by evacuating the tube and flashing the cathode. These localized abnormally hot cathode areas were due to nonuniform cathode cross

section and the cathodes in these tubes eventually burned through at these particular points.

Other discharge oscillations occurred which could be reduced or eliminated by varying the cathode temperature. These oscillations were generally about 200 cycles per second. They were more of a problem in Tubes 3, 4, and 5 than for Tube 2 where the oscillations were not so troublesome. The oscillations tended to modulate the amplitude of the signal transmitted through the plasma, making it quite difficult to get accurate interferometer data.

The geometrical arrangement of Tube 2 with its non-planar cathode and box-like heat shield produced a discharge which appeared to emerge from the back and interior end surfaces of the cathode. This was due to the fact that the back areas of the cathode, being more efficiently shielded, were hotter than the front part, and hence more efficient emitters. As a result, the cathode in Tube 2 was more difficult to activate, and its discharge required a higher anode voltage than Tube 3, though the cathode area of Tube 3 was only half that of Tube 2.

Some typical voltage current (V-I) curves for Tubes 2 through 5 are presented in Figs. III-4 and III-5. Typical ignition and turn-off voltages as a function of pressure are shown in Fig. III-6. The discharge voltage for a given current depended on the discharge mode, as mentioned above, the cathode temperature and the gas pressure. As a result, it was not uncommon during the course of making a data run which lasted an hour or more, to experience a ten per cent change in anode voltage for a given current. A small drop generally took place quite soon after the discharge had been started and a larger decrease occurred after currents of 1 amp or more had been drawn.

Difficulties due to gas cleanup were also encountered and it was manifested by a decrease in the gas pressure as the tube absorbed some of its fill gas. A five per cent drop in the manifold pressure during one-half to one hour data runs was

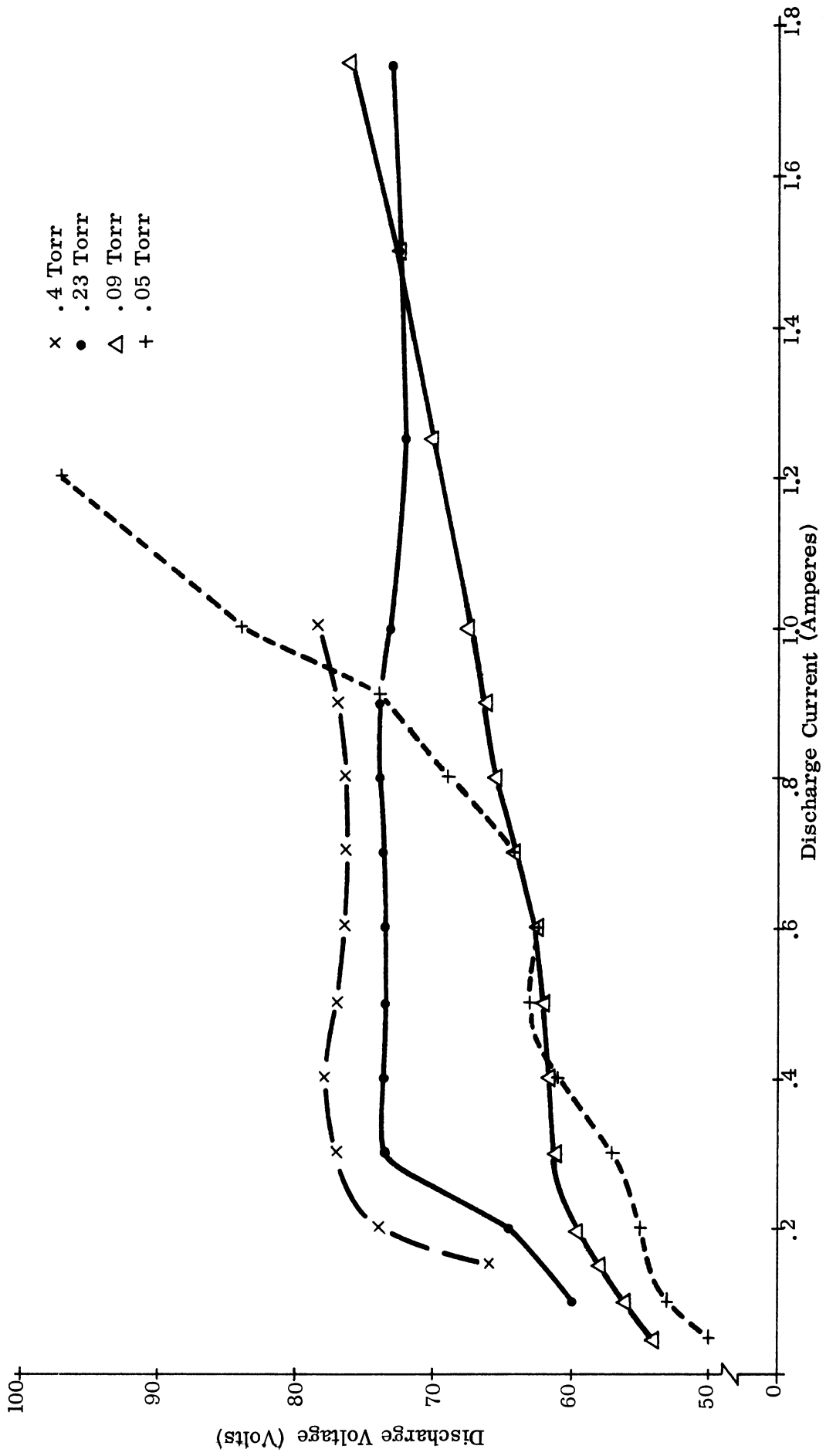


FIG. III-4: VOLTAGE CURRENT CHARACTERISTICS FOR HYDROGEN DISCHARGE IN TUBE 5

Tube	Pressure
2	0.090 Torr
3	0.073 Torr
4	0.098 Torr
5	0.090 Torr

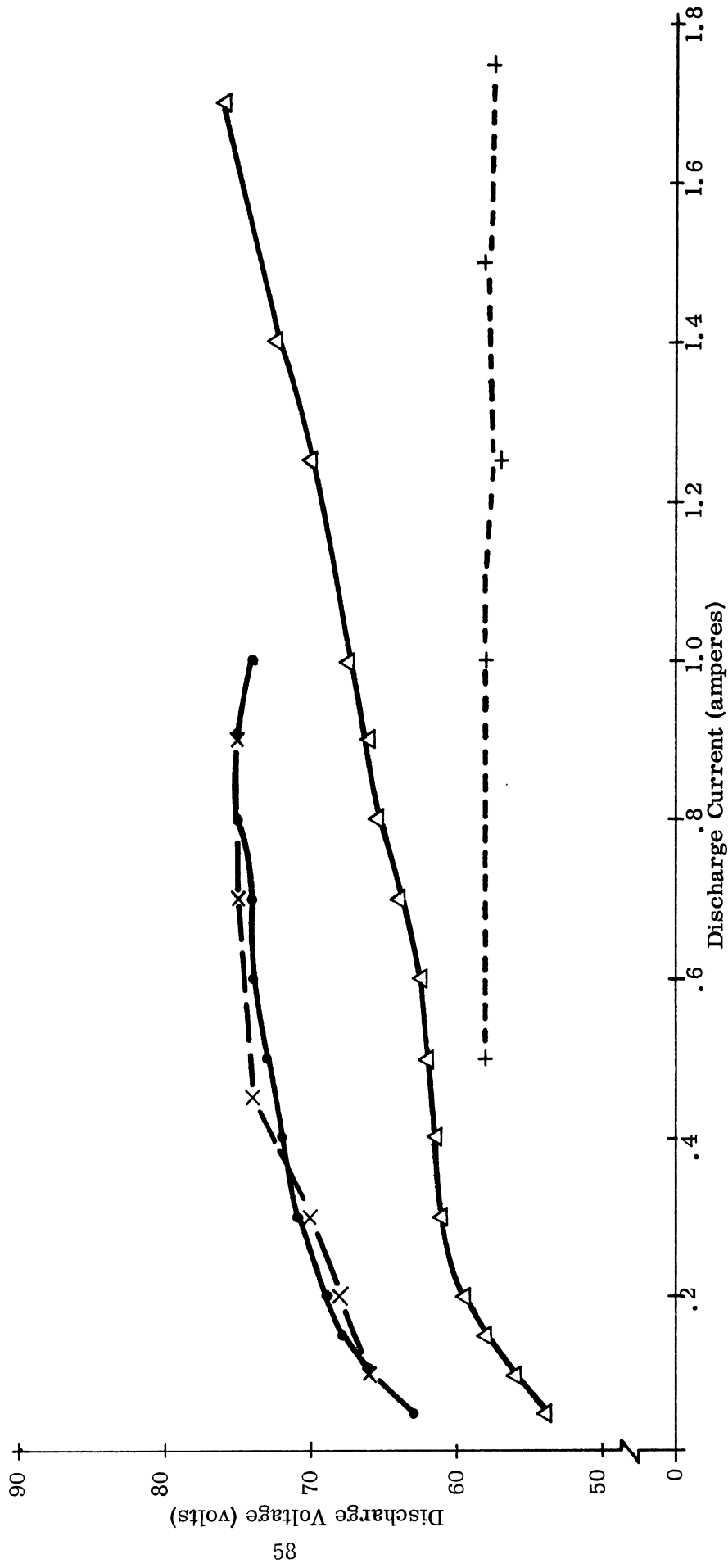


FIG. III-5: VOLTAGE CURRENT CHARACTERISTIC FOR HYDROGEN DISCHARGE

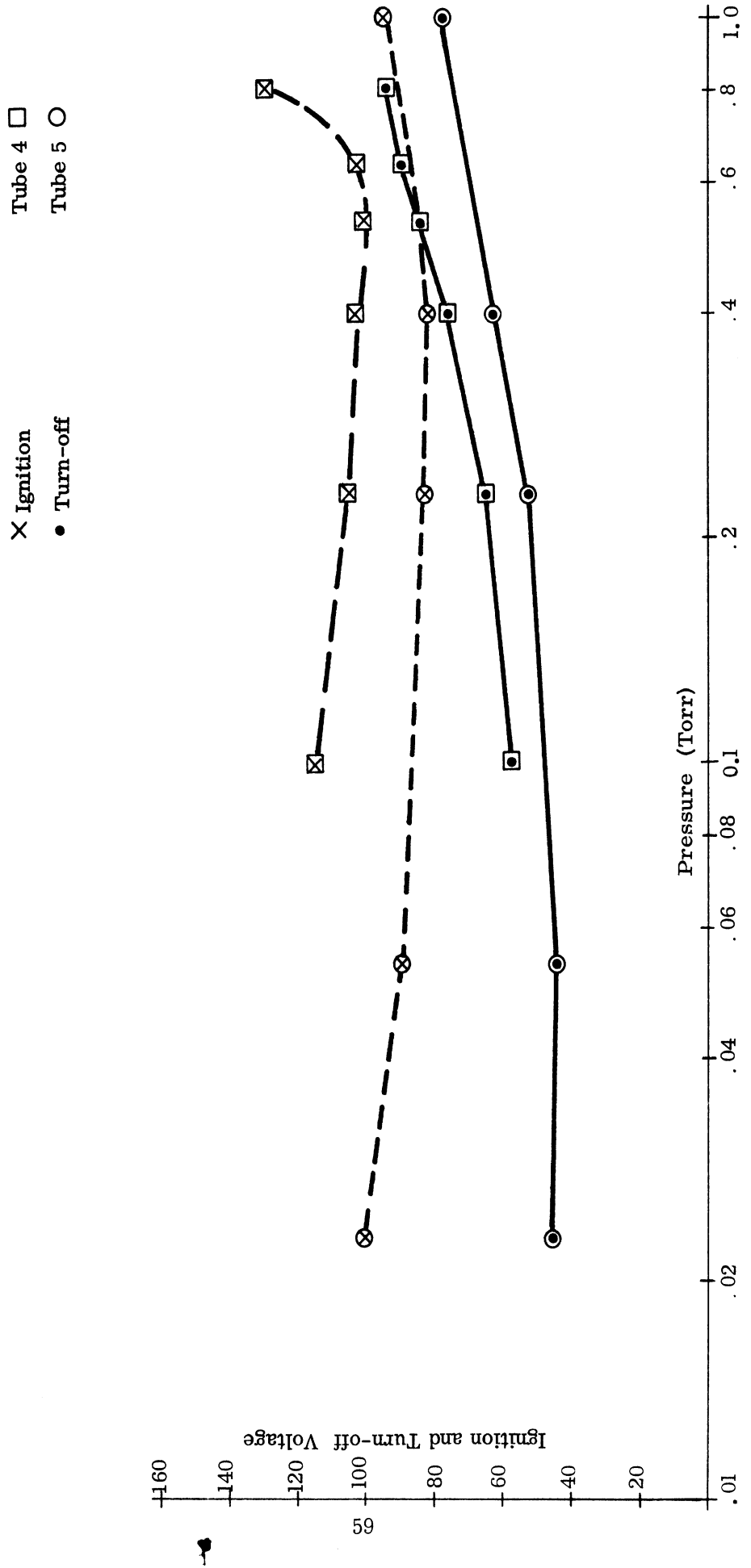


FIG. III-6: IGNITION AND TURN-OFF VOLTAGES FOR HYDROGEN DISCHARGE

usually experienced for pressures less than 0.4 Torr. Since the valve between the plasma tube and vacuum manifold was open during this time, and the manifold has a volume twice that of the envelope this means that the tube absorbed the equivalent of about 15 per cent of its original fill gas. It should be noted that during the course of such a data run, the discharge current was not fixed, but varied between zero and 1 to 3 amps. During a two and one-half hour run at a continuous discharge current of 200 ma, the pressure decrease was about 18 per cent, with a starting pressure of 0.4 Torr.

The voltage required for a given current decreased with decreasing pressure for pressures above 0.1 Torr. The clean-up then could account for the decreasing discharge voltage during a run, at least in part. However, no clean-up was observed for pressures exceeding 0.5 Torr, while the discharge voltage did change at these pressures.

The ratio of the electron plasma frequency to the probing radio frequency, P , obtained from the interferometer measurements is plotted against the square root of the discharge current, $\sqrt{I_d}$, for pressures between 0.1 and 0.8 Torr in Figs. III-7 through III-11. This data was obtained from runs spread over a period of several days, using Tube 4 and a probing frequency of 10.6 Gc. There are two graphs for the pressure 0.4 Torr. The second of these, Fig. III-10 indicates the parameter P for three positions of the receiving horn; close to the cathode, mid-way between cathode and anode, and near the anode.

The spread of the data points is generally within ± 15 per cent at a fixed current and pressure and the grouping is such that the data can be represented by a straight line. This indicates that the electron drift velocity is relatively constant over the current range used. The data shows that the electron plasma frequency is approximately doubled when the pressure is increased from 0.1 to 0.8 Torr and at 0.4 Torr, there seems to be no density gradient between cathode and anode. A

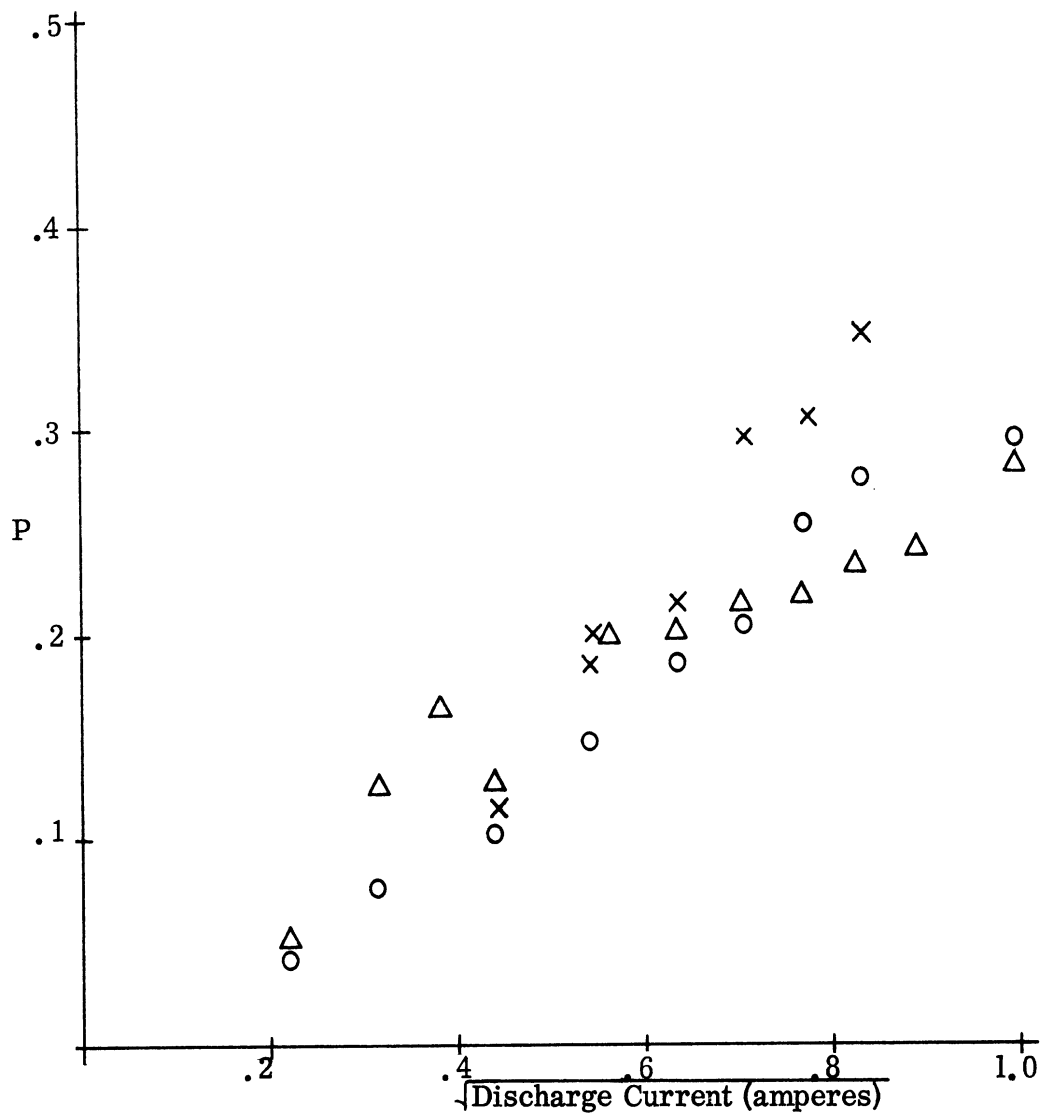


FIG. III-7: NORMALIZED PLASMA FREQUENCY AS FUNCTION OF HYDROGEN DISCHARGE CURRENT IN TUBE 4. PRESSURE = 0.1 TORR.

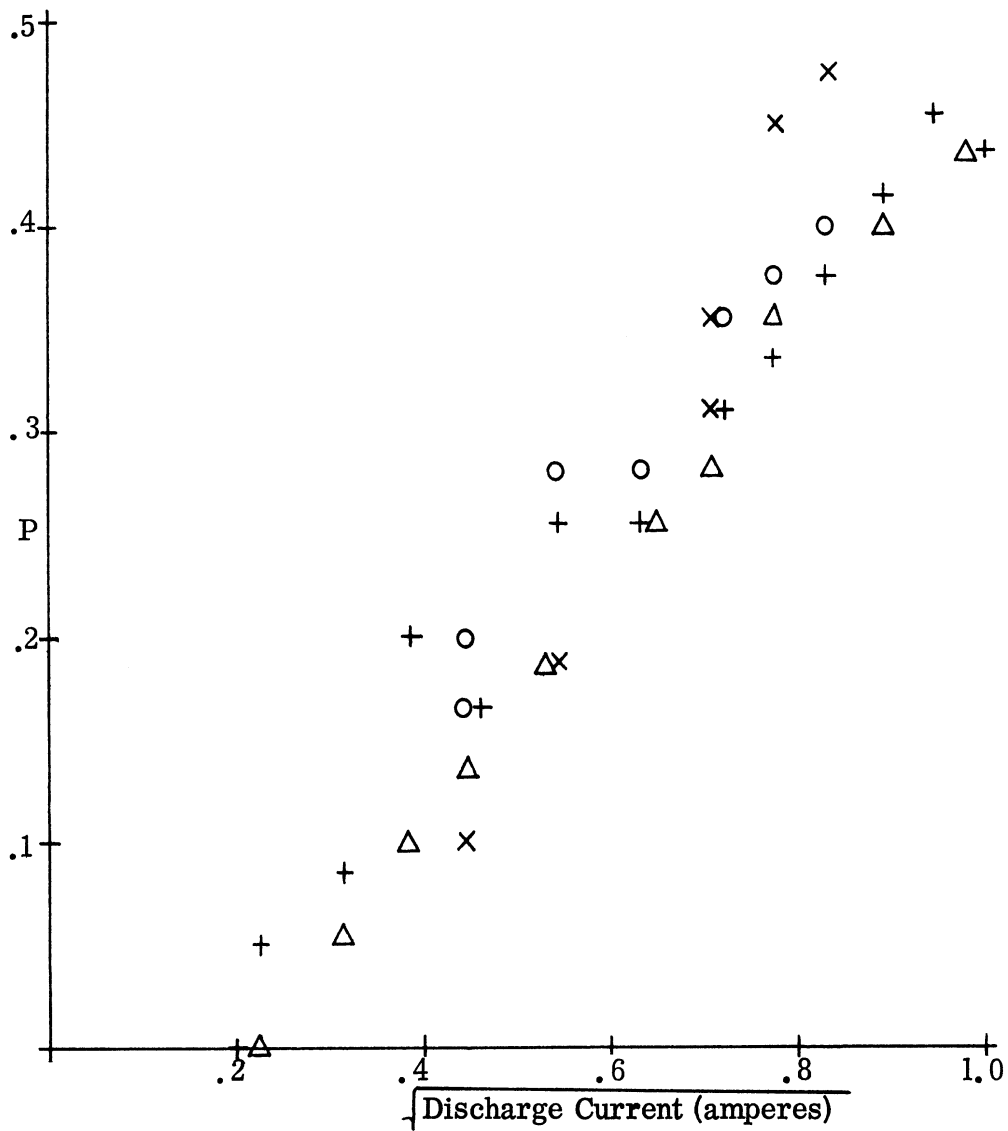


FIG. III-8: NORMALIZED PLASMA FREQUENCY AS A FUNCTION OF HYDROGEN DISCHARGE CURRENT IN TUBE 4. PRESSURE = 0.23 TORR.

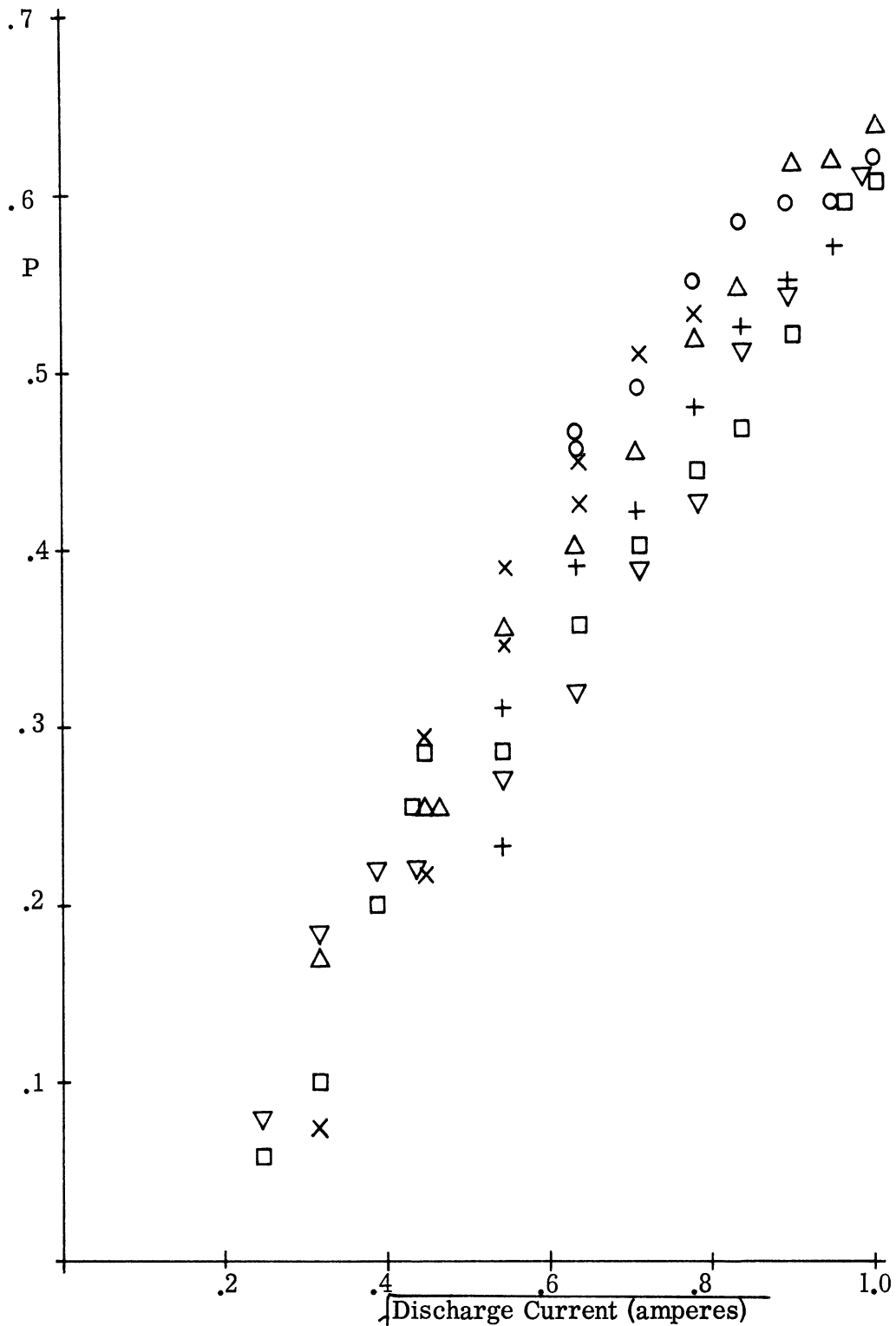


FIG. III-9: NORMALIZED PLASMA FREQUENCY AS A FUNCTION OF HYDROGEN DISCHARGE CURRENT IN TUBE 4. PRESSURE = 0.4 TORR.



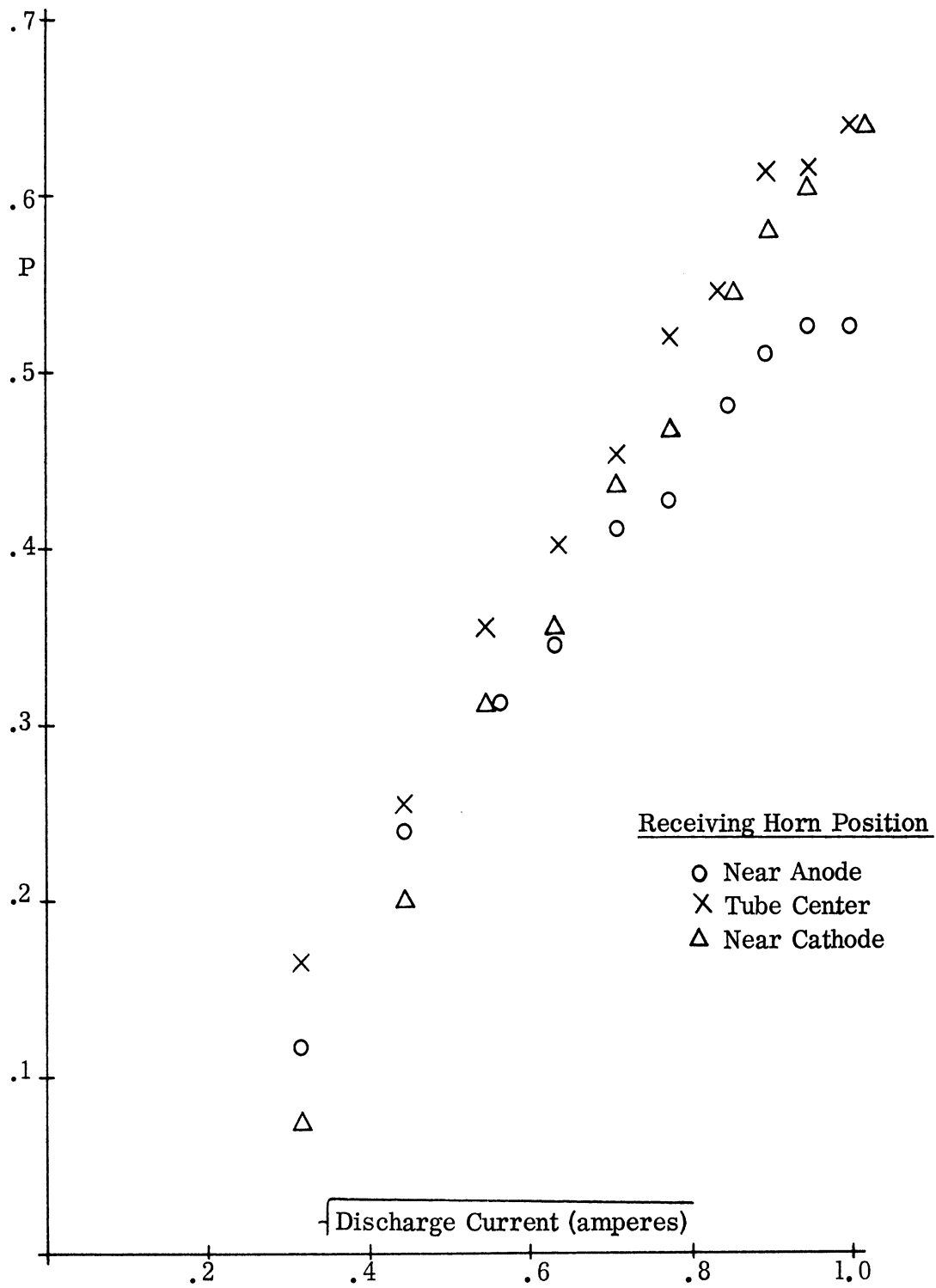


FIG. III-10: NORMALIZED PLASMA FREQUENCY IN HYDROGEN DISCHARGE AT 0.4 TORR AS FUNCTION OF DISCHARGE CURRENT AND POSITION OF RECEIVING HORN FOR TUBE 4.

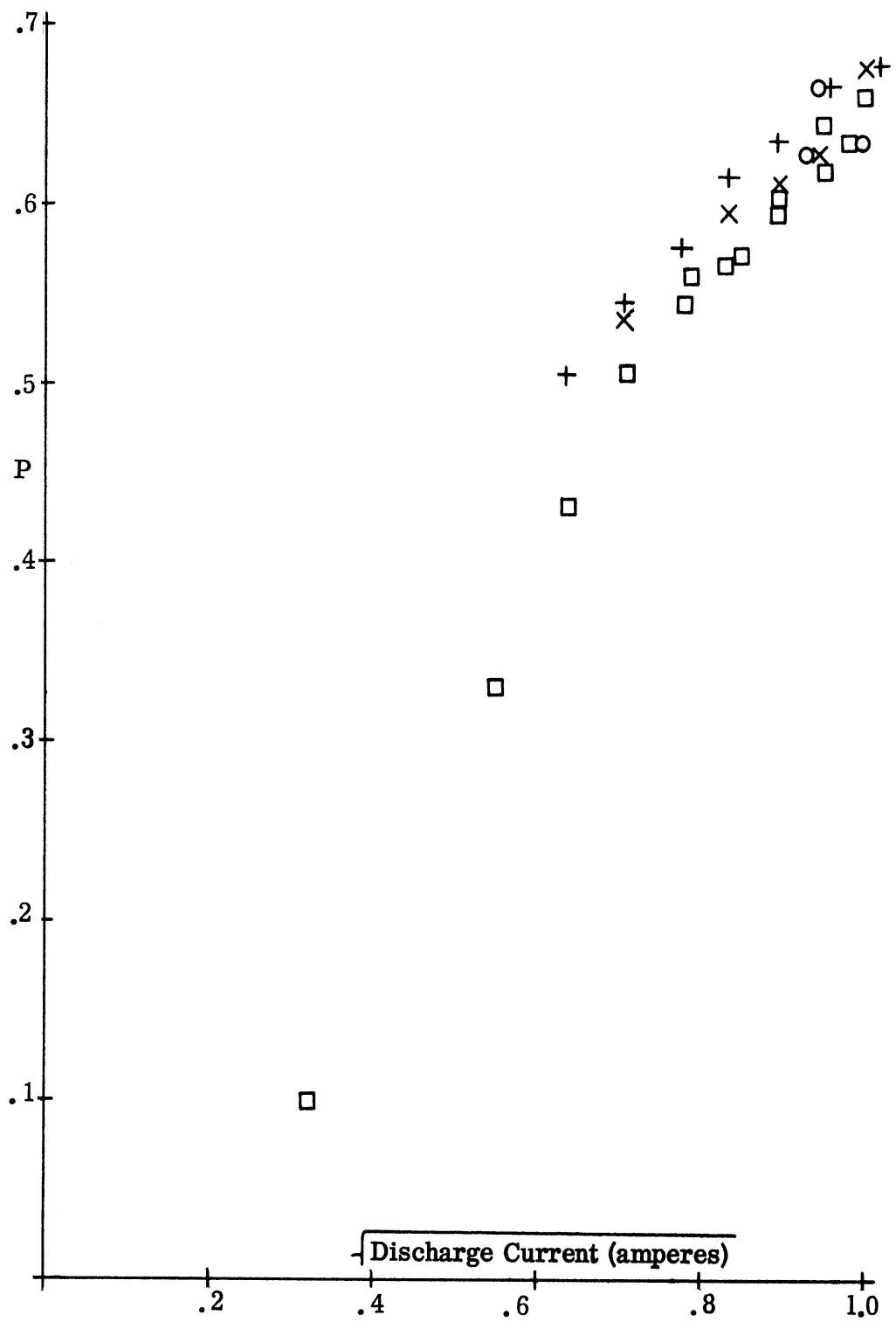


FIG. III-11: NORMALIZED PLASMA FREQUENCY AS FUNCTION OF HYDROGEN DISCHARGE CURRENT IN TUBE 4. PRESSURE = 0.8 TORR

maximum plasma frequency of about 7.0 Gc is obtained at 1 amp. This is more than five times greater than was achieved in a cold cathode argon discharge at 0.13 Torr and 20 ma discharge current (Olte and Miller, 1963). Incorporation of this plasma in the isolator previously discussed would increase the isolation in db by more than 25 times over that obtained by use of the cold discharge, other factors remaining equal.

Xenon Discharge

Data using xenon gas was obtained with Tube 4 and fill pressures of 0.1 to 1.7 Torr. Most of the data was obtained at 0.5 Torr.

The xenon discharge was a deep bluish purple in color and at the lower pressures resembled the low pressure hydrogen discharge. There was a glowing region around the cathode, then a dark space separated from the anode by another glowing region. The discharge was not uniform but consisted of a streamer of glow extending between the cathode and anode. Only as the current approached 1 to 2 amps did the glow form uniformly along the length of the cathode.

Changes in the discharge mode also occurred in xenon. These changes took the form of flickering of the discharge from point to point on the cathode, when the discharge current was low. Corresponding voltage variations also occurred. As the current was increased, the discharge became more stable, and gradually most of the cathode was surrounded by glowing gas. This behavior was observed at all fill pressures used.

More rapid oscillations also took place that could be observed as intensity variations in the brightness of the glow and also were observed in variations of the cathode current and the transmitted power. These oscillations were seen at all pressures.

Some V-I curves for the xenon gas discharge are presented in Fig. III-12. The ignition and turn-off voltage are shown as a function of pressure in Fig. III-13.

- 1.35 Torr
- × .95 Torr
- .5 Torr
- + .25 Torr
- △ .1 Torr

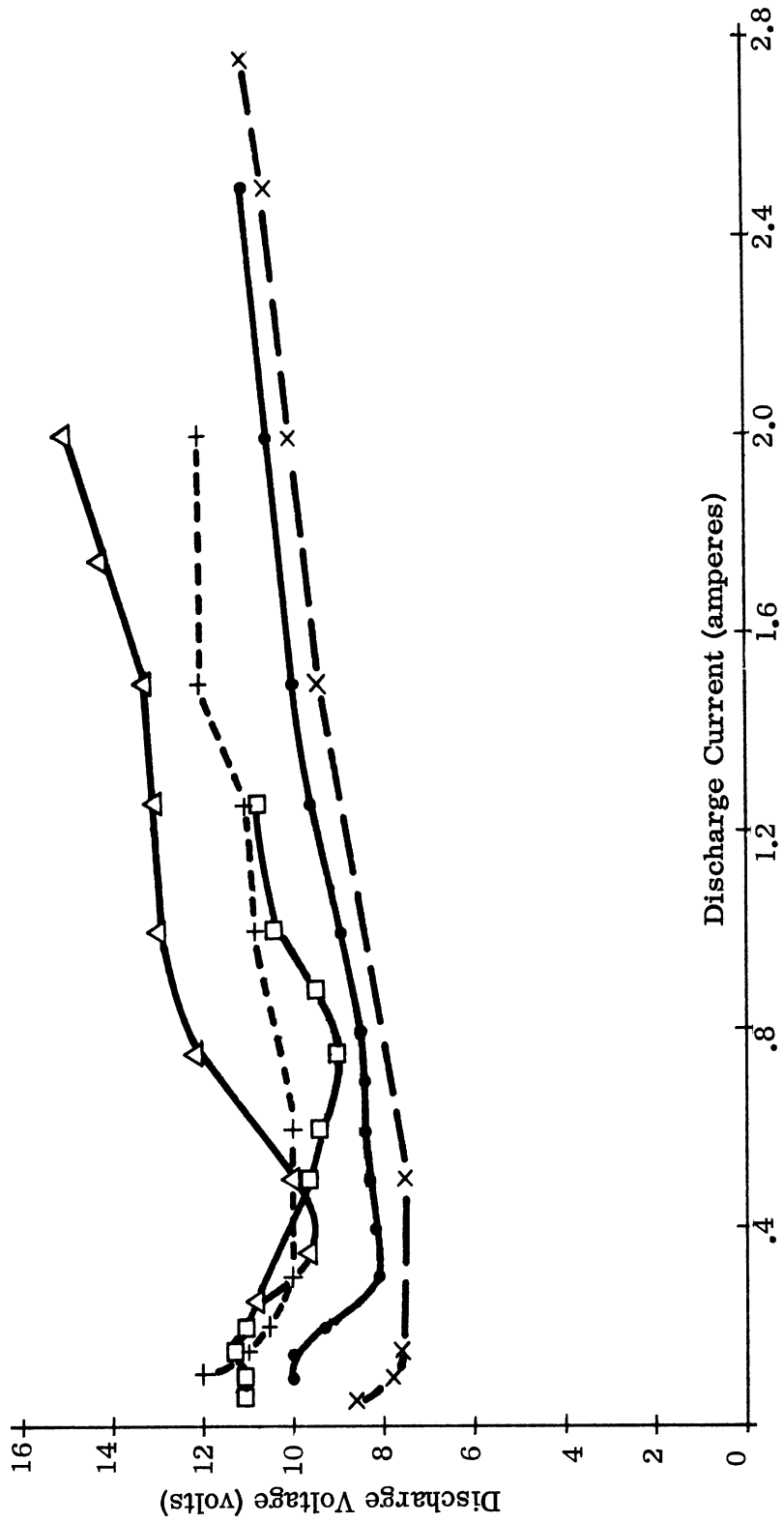


FIG. III-12: VOLTAGE CURRENT CHARACTERISTICS FOR XENON DISCHARGE IN TUBE 4.

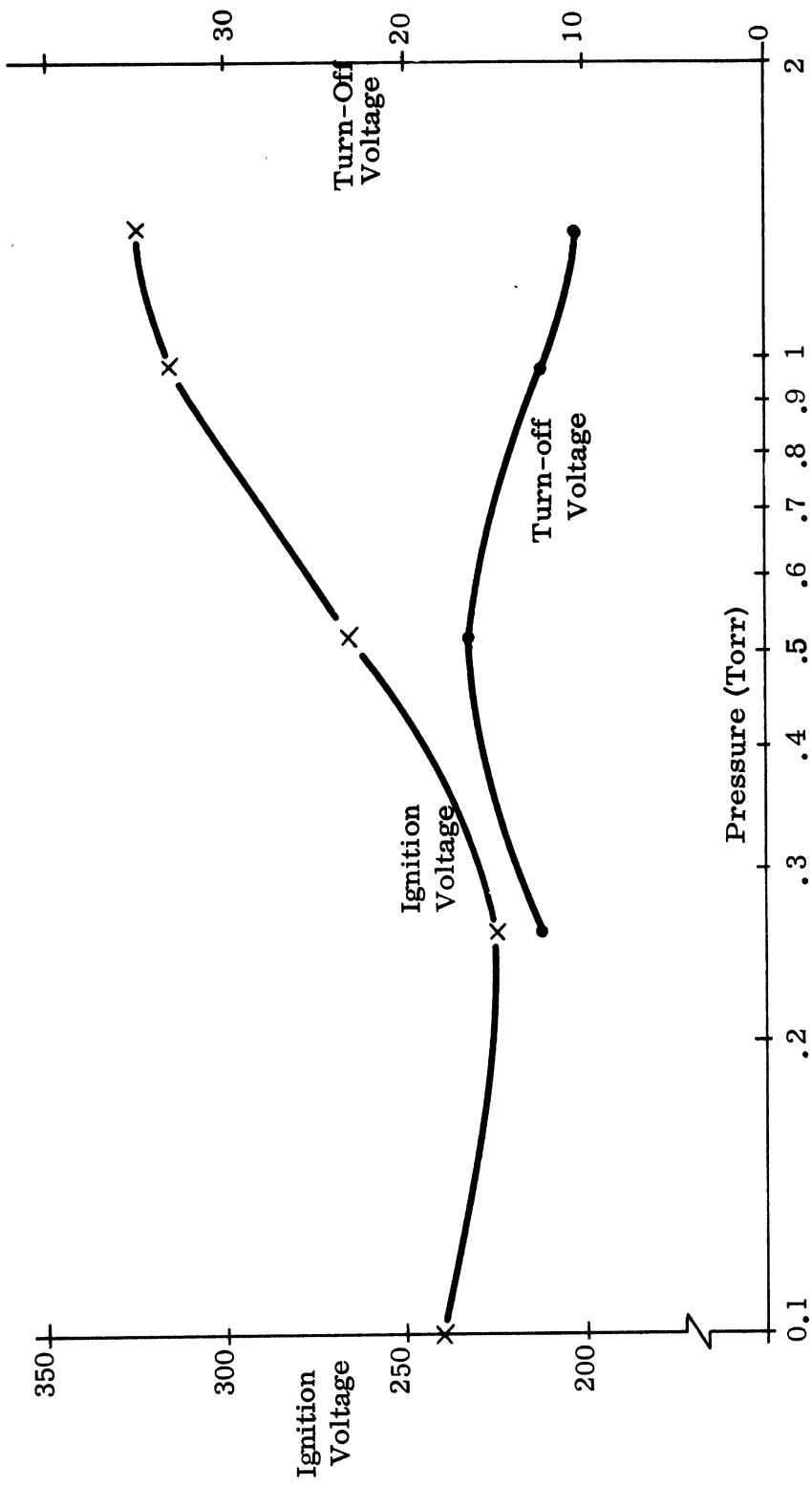


FIG. III-13: IGNITION AND TURN-OFF VOLTAGES FOR XENON DISCHARGE IN TUBE 4.

It is seen that the operating voltage of the xenon discharge is almost $1/10$ that necessary for hydrogen, but that the starting voltages are greater. An operating voltage of about 6.5 volts was at first required for 500 ma discharge current in xenon gas at 0.5 Torr but due to the slow deterioration of the cathode this had risen to 12 to 15 volts when the tube was removed from the manifold.

There was no clean-up problem experienced with the xenon discharge, but rather an increase in pressure while the discharge was in operation. The pressure rise was not noticed consistently nor was it found to occur to any extent at pressures exceeding 1.0 Torr. The maximum change that took place corresponded to a 70 per cent increase in the original fill pressure in a time of one and one-half hours, with a starting pressure of 0.5 Torr.

When experimentation with the xenon discharge was initially begun, it was soon apparent that the electron densities were greater than those for hydrogen and it was seen also that the xenon discharge was considerably more oscillatory. Because of the discharge oscillation, an attempt was made to make interferometer measurements at the maximum discharge current. This was accomplished by observing the transmitted wave form on a synchroscope and nulling the signal wave form pattern at the point which corresponded to the maximum current. The higher electron densities produced enough attenuation so that the magnitude of the power transmission coefficient could be used for a determination of the electron density, rather than relying on the phase shift alone. Data was also obtained by taking an average null point which corresponded to the average current when the oscillations were not too severe. The heater current was changed to dc from ac in an attempt to decrease the oscillations, but this had no apparent effect upon them.

In Figs. III-14, III-15 and III-16 some results are presented which show the parameter P as a function of the square root of the discharge current. The un-enclosed points are computed from phase measurement, and the enclosed ones are

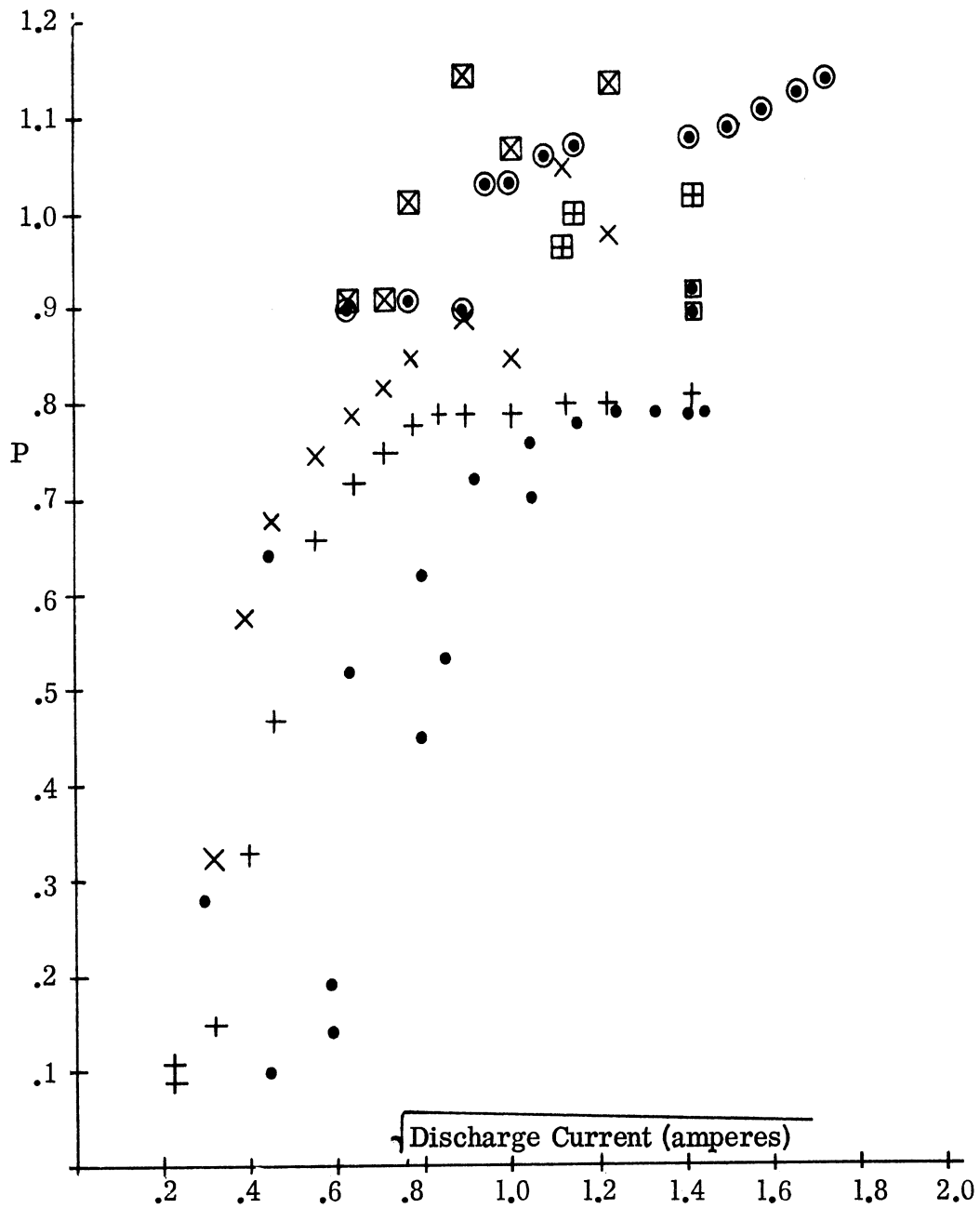


FIG. III-14: NORMALIZED PLASMA FREQUENCY AS A FUNCTION OF XENON DISCHARGE CURRENT IN TUBE 4. PRESSURE = 0.25 TORR.

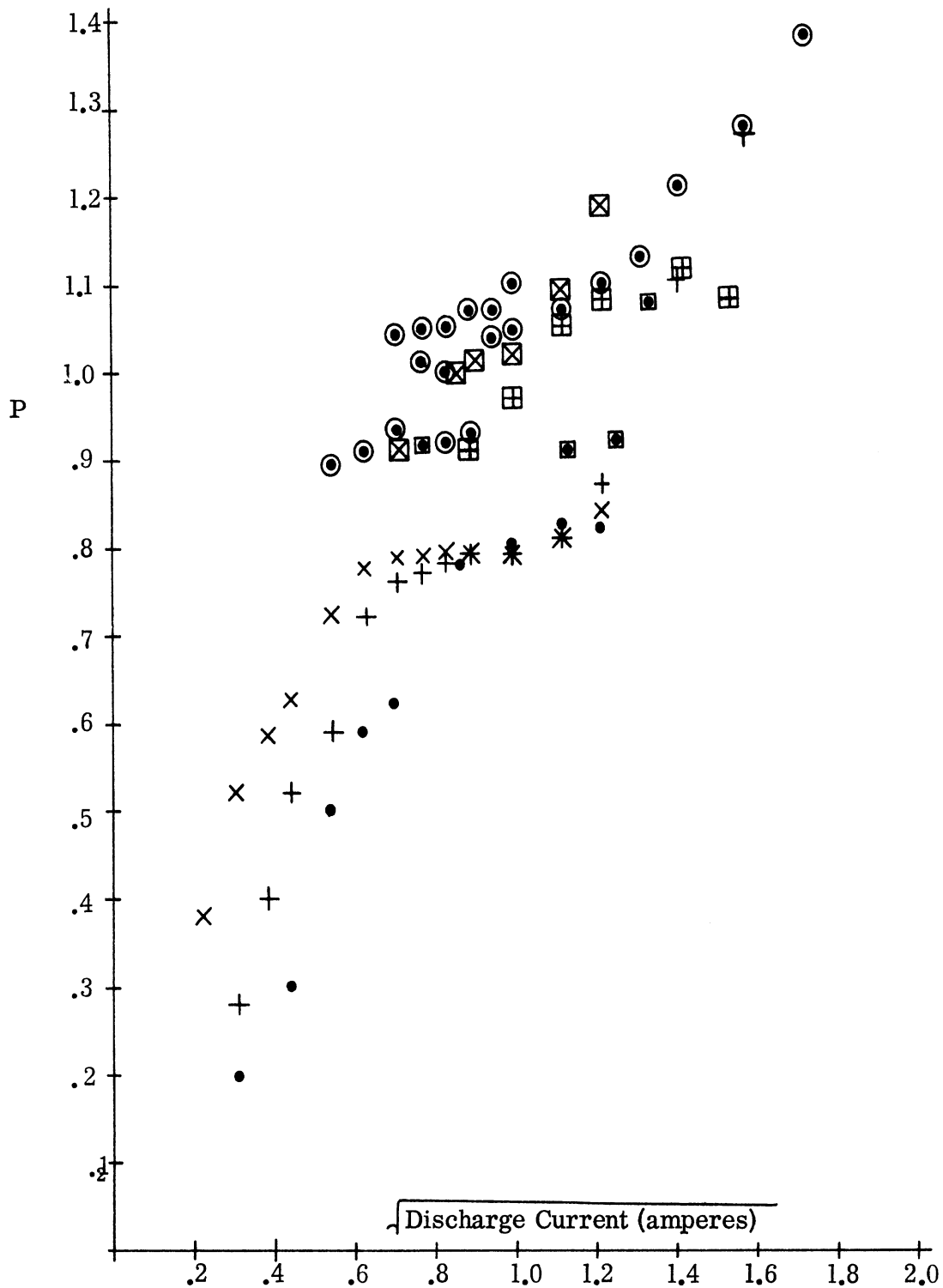


FIG. III-15: NORMALIZED PLASMA FREQUENCY AS A FUNCTION OF XENON DISCHARGE CURRENT IN TUBE 4. PRESSURE = 0.5 TORR.

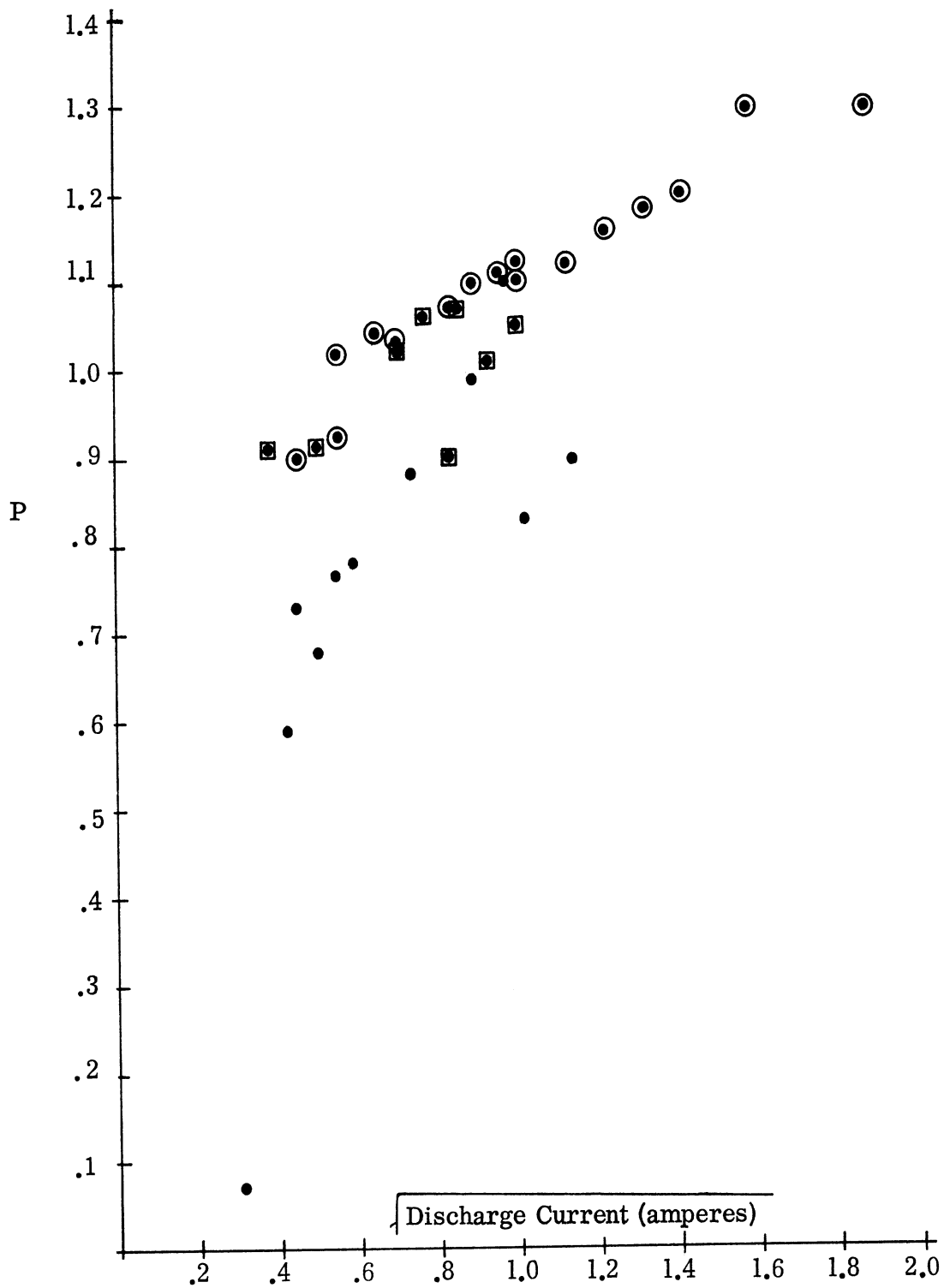


FIG. III-16: NORMALIZED PLASMA FREQUENCY AS A FUNCTION OF XENON DISCHARGE CURRENT IN TUBE 4. PRESSURE = 1.17 TORR.

from attenuation measurement. Dots are used to indicate that the measurement was made when the discharge current oscillation was at a maximum, while + and x indicate average discharge current.

There is a considerably greater spread in these results than those obtained using hydrogen. In addition, there is some disagreement between results obtained from the attenuation and phase shift measurements. In general, the P values from phase shift data is less by 20 or 30 per cent than from the attenuation data for the same current.

The discrepancy between the phase and attenuation data could be due to a small, but finite electron collision frequency. With a ratio of 0.1 for collision frequency to probing frequency the phase shift across the plasma would be affected only slightly but there would be an appreciable increase in the attenuation, as P approaches unity. This would result in overestimating the value of P when assuming there are no collisions. Since the collision frequency is pressure dependent, the disagreement between the phase and attenuation data should be also, but this does not seem to be the case.

The fact that the phase shift data produces on the average, nearly a straight line relationship between P and the square root of the discharge current up to a value for P of about 0.75 and then exhibits a sharp discontinuity, indicates that the model may be inadequate for P values beyond this. This could account for the difference in the phase and attenuation data also.

We note that for $\sqrt{I_d}$ less than 0.5 at the pressure of 0.25 Torr there may be a difference in P values of more than three times at the same current. It was found in particular that data taken on runs when the discharge current was being increased and when it was being decreased, was generally different. The greatest discrepancy occurred at low discharge currents, when the discharge consisted of a glowing streamer of gas between cathode and anode and did not fill the tube volume. The position of the streamer was variable. This inhomogeneity of the discharge

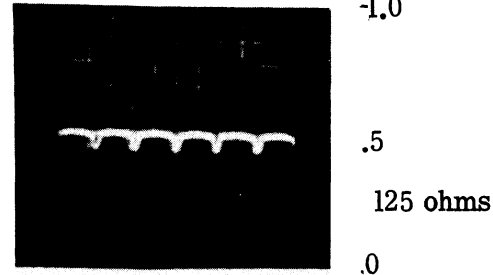
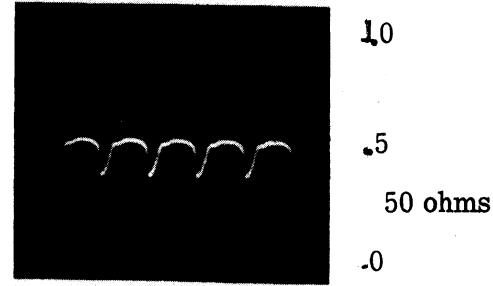
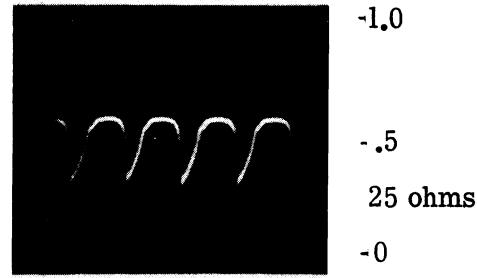
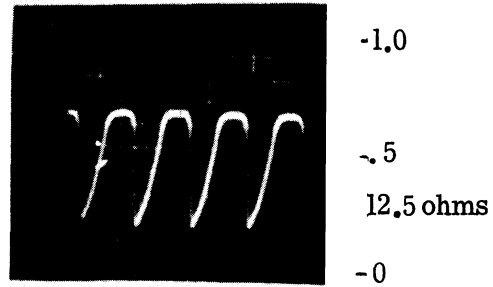
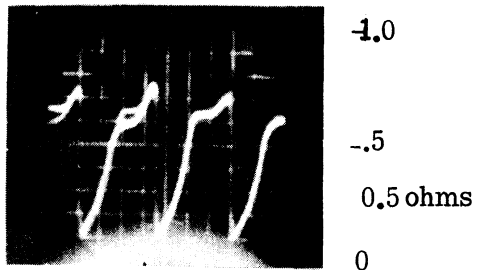
provides the most likely cause for the scatter in the data points.

If we extrapolate the xenon data to 1 amp discharge current at .5 Torr, we obtain a value of about 1.1 for P , or a plasma frequency of almost 12 Gc. This exceeds the hydrogen discharge plasma frequency at the same current by more than 50 per cent. An additional advantage of the xenon discharge is that it requires only about one tenth the anode voltage as is required for the hydrogen discharge. Thus, for a given plasma frequency, the discharge power required would be about $1/18$ for the xenon discharge compared with the hydrogen. This works out to about $f_p^2/12$ watts, in the xenon discharge and $1.6 f_p^2$ watts in hydrogen for the discharge power at 0.5 Torr pressure, when f_p is given in Gc.

The main disadvantages of the xenon discharge are its inhomogeneity, primarily at currents less than 1 amp, and the oscillations which were previously mentioned. The oscillation amplitude was found to be very sensitive to the resistance in the anode circuit. The frequency varied between 200 and 1300 cycles per second, decreasing as the pressure increased. Fig. III-17 shows the current and transmitted power wave forms as the external resistance is varied, for a pressure of 0.4 Torr.

In summary, the experimental phase of this investigation has shown that significantly higher plasma frequencies, higher by a factor of 5 to 10, are obtainable in the hot cathode discharge than with the cold discharge. This advantage was expected, but the disadvantage encountered with the stability of the hot discharge plasma was not anticipated. The oscillatory nature of the discharge can not be eliminated altogether, but the problem may be alleviated by changes in the cathode assembly to insure more uniform cathode temperatures, by the use of a grid to apply a negative feedback to the discharge current, or by control of the external elements connected in the discharge circuit. The long-term stability of the discharge is limited by cleanup of the fill gas, and cathode deterioration, and of these two items,

Current Waveform Horizontal 2ms/div. Vertical 0.1 amr/div.



Transmitted Power Waveform Horizontal 10 ms total. Vertical 0, -3, -10, -15 db lines

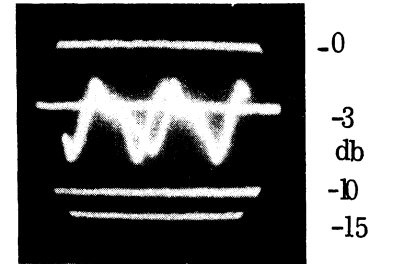
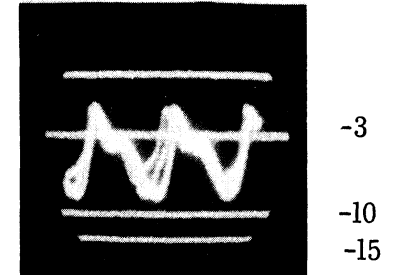
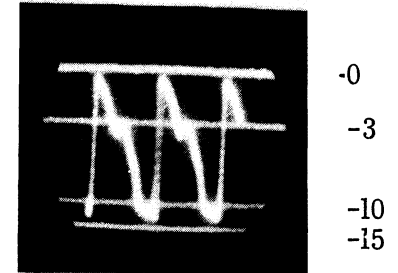
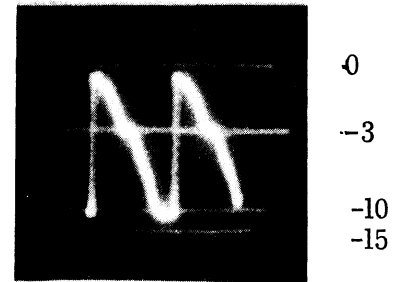
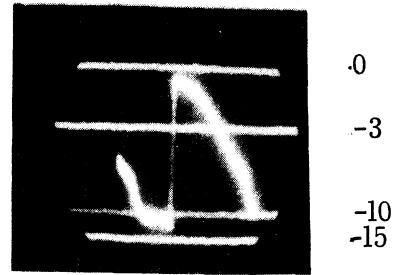


FIG. III-17: MODULATION OF TRANSMITTED RF POWER AND DISCHARGE CURRENT BY PLASMA OSCILLATION IN XENON GAS AT 0.4 TORR

the first is the more serious. Our experience has indicated that the clean-up in hydrogen gas becomes less significant when the fill pressure is increased, so that perhaps a reserve could be designed into the discharge tube.

The most serious problem in building a plasma package of this shape appears to be encountered in the glass envelope, not in its fabrication, but in the addition of the cathode and anode sub-assemblies. The peculiar shape of the envelope requires that it be annealed, but this cannot be done after the cathode has been added. As a result, stresses are set up in the glass which frequently led to cracking of the envelope. This problem can probably be solved with some changes in the design. It thus appears that a convenient plasma package of reasonably high electron density can be obtained using the hot cathode discharge, although the stability is less than desired.

IV CONCLUSIONS

The successful application of a plasma in a microwave circuit requires that one utilize a plasma property which is sufficiently stable for the intended component. The electron gyro-frequency is an example which is dependent only on the external static magnetic field applied to the plasma, and as such, is independent of changes in the plasma. This has been made use of in a microwave isolator, a device dependent on the interaction of the TM_{11} mode, e. g. in a waveguide with plasma electron density subject to an external static magnetic field. A first order theory which has been developed for the microwave isolator has been compared with some experimental results. Comparison of the theory and experiment indicates that the theory is reasonable when the main assumptions on which it is based, are satisfied by the experimental conditions.

The problem of making a rectangular plasma package using a hot cathode has been investigated. The investigation has not been carried to the desired stage of development, particularly with respect to both long and short term plasma stability. A primary advantage of the hot cathode discharge is the higher plasma frequency which may be obtained, i. e. 10 Gc or more. The principal shortcoming appears to be the plasma instability which arises from plasma oscillations, gas clean-up, and aging of the cathode. A planar cathode does not seem to reduce the plasma oscillations appreciably.

In any further work in this area, the primary effort should be to obtain a stable plasma package whose properties may be varied in a desirable manner. Before this can be done, a better understanding of the collective plasma processes themselves is mandatory. In such a study, attention should be given to the electron

and ion acoustical waves and their coupling to the discharge current. The influence of the plasma sheath on this coupling should also receive some further attention. When the plasma package is immersed in a static magnetic field then a similar problem involves a study of the magneto-hydrodynamic wave interaction with the discharge current and the plasma sheath insofar as it affects the plasma package oscillations.

REFERENCES

- Bachynski, M. P. , G. G. Cloutier and K. A. Graf (1963) "Microwave Measurements of Finite Plasmas, " RCA Victor Research Laboratory Report 7-801-26.
- Collin, R. E. (1960) Field Theory of Guided Waves, McGraw-Hill Book Company, New York, pp 244-247.
- Maddix, H. S. , J. Gregory and C. S. Ward (1963) "Investigation of High Power Gaseous Electronics, " Microwave Associates, Contract No. DA-36-039-AMC-00097 (E).
- Maddix, H. S. , C. S. Ward (1962) "Investigation of High Power Gaseous Electronics, " Microwave Associates, Final Progress Report, Contract No. DA-36-039-SC-89161.
- Olte, A. , and E. K. Miller (1963), "A Study of Plasma Applications in Microwave Circuits, " The University of Michigan Radiation Laboratory Report 4915-1-F, RADC-TDR-63-54, AF 30(602)-2605.
- Ramo, S. and J. R. Whinnery (1960) Fields and Waves in Modern Radio, John Wiley and Sons.

